Dietary sulfur amino acid restriction improves glucose homeostasis through hepatic *de novo* serine synthesis

Andres F. Ortega[1], Cha Mee Vang[1], Ferrol I. Rome[1], Kaitlyn M. Andreoni[2], Aiden M. Phoebe[2], Alisa B. Nelson[1], Peter A. Crawford[1,3], James J. Galligan[2], Stanley Ching-Cheng Huang[4,5], Curtis C. Hughey[1]*

[1]Division of Molecular Medicine, Department of Medicine, University of Minnesota, Minneapolis, MN

[2]Department of Pharmacology and Toxicology, University of Arizona, Tucson, AZ

[3]Department of Biochemistry, Molecular Biology, and Biophysics, University of Minnesota, Minneapolis, MN

[4]Pelotonia Institute for Immuno-oncology, Comprehensive Cancer Center – James Cancer Hospital and Solove Research Institute, The Ohio State University, Columbus, OH

[5]Department of Microbial Infection and Immunity, College of Medicine, The Ohio State University, Columbus, OH

*To whom the correspondence should be addressed: Curtis C. Hughey from the Department of Medicine, Division of Molecular Medicine, University of Minnesota, Dwan 316, 425 East River Parkway, Washington Ave SE, Minneapolis, MN, 55455. Tel.: 612-301-2677, Email: chughey@umn.edu

ABSTRACT

Dietary sulfur amino acid restriction (SAAR) improves whole-body glucose homeostasis, elevates liver insulin action, and lowers liver triglycerides. These adaptations are associated with an increased expression of hepatic *de novo* serine synthesis enzymes, phosphoglycerate dehydrogenase (PHGDH) and phosphoserine aminotransferase 1 (PSAT1). This study tested the hypothesis that enhanced hepatic serine synthesis is necessary for glucose and lipid adaptations to SAAR. Hepatocyte-specific PSAT1 knockout (KO) mice and wild type (WT) littermates were fed a high-fat control or SAAR diet. In WT mice, SAAR increased liver PSAT1 protein (~70-fold), serine concentration (~2-fold), and ^{13}C-serine (~20-fold) following an intravenous infusion of [U-^{13}C]glucose. The elevated liver serine and partitioning of circulating glucose to liver serine by SAAR were attenuated in KO mice. This was accompanied by a blunted improvement in glucose tolerance in KO mice fed a SAAR diet. Interestingly, SAAR decreased liver lysine lactoylation, a SAA-supported post-translational modification known to inhibit PHGDH enzymatic activity. This suggests dietary SAAR may increase serine synthesis, in part, by lowering lysine lactoylation. Beyond glucose metabolism, dietary SAAR reduced body weight, adiposity, and liver triglycerides similarly in WT and KO mice. Collectively, these results demonstrate that hepatic PSAT1 is necessary for glucose, but not lipid, adaptations to SAAR.

KEYWORDS

Sulfur amino acid restriction; De novo serine synthesis; Glucose homeostasis; Liver intermediary metabolism

47 **1. INTRODUCTION**

48 Dietary sulfur amino acid restriction (SAAR) provokes metabolic adaptations that are
49 advantageous in preventing and treating obesity and its comorbidities [1]. In rodents, SAAR
50 enhances glucose and insulin tolerance [2-7]. The use of hyperinsulinemic-euglycemic clamps
51 combined with isotope tracers revealed that the increased insulin action is due to a greater
52 suppression of endogenous glucose production and heightened glucose disposal by skeletal
53 muscle, heart, and adipose tissue [8-11]. Concurrently, SAAR decreases adiposity and liver
54 triglycerides [1-4]. It is important to note that these metabolic responses to SAAR are not confined
55 to rodents. Short-term dietary SAAR in humans elicits decreases in body weight, body mass index
56 (BMI), and liver fat [12-14]. The SAAR-mediated adaptations are partly due to a liver-derived
57 increase in fibroblast growth factor 21 (FGF21) [1]. The transcriptional activation of hepatic
58 FGF21 increases whole-body energy expenditure, which contributes to reduced adiposity by
59 SAAR [9]. FGF21 is necessary for the enhanced insulin-stimulated cardiac glucose uptake [10;
60 11]. In contrast, SAAR lowers liver triglycerides similarly in wild type (WT) and FGF21-deficient
61 mice[9]. Prior work indicates the enhanced liver insulin signaling by SAAR is also independent of
62 FGF21 [1; 11]. Together, these findings suggest that the increased FGF21 mediates several
63 extrahepatic responses to SAAR, but may not be critical for the hepatic responses. Given this, the
64 mechanisms underlying the liver glucose and lipid adaptations to SAAR, and the extent to which
65 these responses are hepatocyte-dependent, remain to be clearly defined.

66 Elevated expression of liver *de novo* serine synthesis pathway enzymes, phosphoglycerate
67 dehydrogenase (PHGDH) and phosphoserine aminotransferase 1 (PSAT1), is among the most
68 reproducible responses to dietary SAAR, making their increase a marker of a successful dietary
69 intervention [2; 9; 10; 15-23]. *De novo* serine synthesis is sourced from 3-phosphoglycerate, an

70 intermediate of both glycolysis and gluconeogenesis [24]. Thus, a SAAR-mediated increase in
71 hepatic serine synthesis could promote greater glucose disposal and/or divert gluconeogenic flux
72 away from glucose production. Liver-specific PHGDH knockout (KO) mice fed a chow diet show
73 higher adiposity and reduced glucose tolerance [25]. In agreement with PHGDH KO mice, PSAT1
74 knockdown impairs glucose and insulin tolerance [26]. Conversely, PSAT1 overexpression
75 enhances glucose and insulin tolerance [26]. Beyond glucose homeostasis, the overexpression of
76 PHGDH has been shown to lower liver lipids [27]. These prior results support that PHGDH and
77 PSAT1 action impacts whole-body and liver-specific glucose and lipid homeostasis.

78 The experiments presented herein tested the hypothesis that hepatic PSAT1 is required for
79 the liver glucose and lipid adaptations to SAAR to be fully realized. Liver-specific PSAT1 KO
80 mice and WT littermates were fed a high-fat control or SAAR diet. Comprehensive phenotyping
81 approaches were completed. These included glucose and insulin tolerance tests to define whole-
82 body glucose homeostasis, ^{13}C-isotope tracing in conscious unrestrained mice to determine the
83 tissue-specific fate of glucose and serine *in vivo*, and metabolomics to quantify metabolite
84 concentrations. Immunoblotting and proteomics were used to identify molecular drivers of liver
85 metabolism. The results of this study show that hepatic PSAT1 is necessary for whole-body and
86 liver-specific glucose, but not lipid, adaptations to dietary SAAR.

87

88 **2. MATERIALS AND METHODS**

89 *2.1. Mouse models and husbandry*

90 All procedures using mice were approved by the University of Minnesota Institutional
91 Animal Care and Use Committee. PSAT1 floxed mice on a C57BL/6N background [28] were
92 backcrossed onto a C57BL/6J background for 5 generations. Hepatic-specific PSAT1 KO were

then generated by breeding mice expressing Cre recombinase under control of the albumin promoter (B6.Cg-Tg(Alb-cre)21Mgn/J) with PSAT1 floxed mice on a C57BL/6J background. Floxed PSAT1 littermates lacking expression of Cre recombinase were used as WT controls. C57BL/6J mice were used for select studies. Mice were maintained on a chow diet (Teklad Global 18% Protein Rodent Diet 2918, Madison, WI) from weaning at three weeks of age until six weeks of age. At six weeks of age mice received one of three diets (unless otherwise stated): low-fat SAA control (0.85% kcal from methionine; 10% kcal from fat; LF-CTRL; A11051302B, Research Diets Inc., New Brunswick, NJ), high-fat SAA control (0.85% kcal from methionine; 60% kcal from fat; HF-CTRL; A11051306, Research Diets Inc., New Brunswick, NJ), and HF-SAAR (0.125% kcal from methionine; 60% kcal from fat; A11051305, Research Diets Inc., New Brunswick, NJ). The full dietary composition for these three diets is detailed in Supplementary Table 1. Food and water were provided ad libitum. Mice were housed with cellulose bedding (Cellu-nest™, Shepherd Specialty Papers, Watertown, TN) in temperature- and humidity-controlled conditions maintained on a university instituted 14:10 hour light:dark cycle. At 12 weeks of age (6 weeks on diet), mice underwent metabolic testing and were euthanized via cervical dislocation. Tissues were rapidly excised, freeze-clamped in liquid nitrogen, and stored at -80°C. One cohort of mice was euthanized at 26 weeks of age (20 weeks on diet) using the same procedures described above. All mice used in this study were males.

2.2. Body Composition

Body composition was measured in mice fed ad libitum at 10-11 weeks of age using an EchoMRI-100™ Body Composition Analyzer (EchoMRI LLC, Houston, TX).

116 *2.3 Glucose and insulin tolerance tests*

117 For glucose tolerance tests (GTT), mice were fasted for five hours and injected
118 intraperitoneally (i.p.) with dextrose (Hospira, Inc., Lake Forest, IL) at a dose of 2 $g \cdot kg^{-1}$ lean
119 weight. For insulin tolerance tests (ITT), mice were fasted for five hours and received insulin
120 (Humulin R human, Eli Lilly and Company, Indianapolis, IN) i.p. at a dose of 0.75 $U \cdot kg^{-1}$ lean
121 weight. During both procedures, tail-blood glucose was measured at 0, 15, 30, 45, 60, 90, and 120
122 minutes with a Contour blood glucose meter (Ascensia Diabetes Care, Parsippany, NJ). A cohort
123 of mice had blood samples obtained at 0 and 15 minutes after the insulin administration for plasma
124 insulin concentrations and were euthanized immediately after for assessing indices of insulin
125 signaling in tissues.

126

127 *2.4. Insulin pellet implantation.*

128 At 7 weeks of age, C57BL/6J mice had one sustained-release insulin pellet implanted
129 subcutaneously (~0.1 U/day per implant; LinBit; LinShin Canada, Toronto, ON) according to
130 manufacturer guidelines. Briefly, under isoflurane anesthesia, a 1 cm diameter area of hair was
131 clipped and disinfected. A small incision in the skin was made with a 16-gauge needle, and a sterile
132 12-gauge trocar was used to deliver the pellet subcutaneously. Procedures in control mice were
133 identical, except the skin incisions were not performed. Mice were group housed following the
134 procedure.

135

136 *2.5. Vascular catheter surgeries*

137 At 11 weeks of age, C57BL/6J mice had catheters were surgically implanted in the jugular
138 vein and carotid artery for isotope infusion and sampling protocols as previously described [21;

139 29]. The exteriorized ends of the implanted catheters were flushed with 200 $U \cdot mL^{-1}$ heparinized
140 saline and sealed with stainless-steel plugs. Following surgery, mice were housed individually and
141 provided 5-7 days of post-operative recovery prior to stable isotope infusion studies. Liver-specific
142 PSAT1 KO and WT littermates underwent identical surgical procedures with the exception that
143 only the jugular vein catheter was implanted. All mice were within 10% of pre-surgical weight
144 prior to stable isotope infusions.
145
146 *2.6. Stable-isotope tracing: [U-^{13}C]glucose intravenous infusion in the conscious, unrestrained*
147 *mouse*
148 During the first hour of the housing light cycle, both food and water were withdrawn for
149 the duration of the experiment (5.5 hours). Four hours into the fast, the exteriorized vascular
150 catheters were connected to infusion syringes. Following a one-hour acclimation, a 60 $mg \cdot kg^{-}$
151 $^{1} \cdot min^{-1}$ continuous intravenous infusion of [U-^{13}C]glucose was performed for 30 minutes.
152 C57BL/6J mice had arterial samples obtained for measuring blood glucose prior to and every 10
153 minutes during the [U-^{13}C]glucose infusion to ensure the infusion rate was sufficient to achieve
154 glucose concentrations comparable to those observed during a GTT. Mice were euthanized and
155 tissue collected immediately following the [U-^{13}C]glucose infusion.
156
157 *2.7. Stable-isotope tracing: In-vivo [U-^{13}C]serine intraperitoneal injection*
158 Food and water were withdrawn for 5 hours starting within the first hour of the light cycle.
159 [U-^{13}C]serine was administered i.p. at a dose of 100 $mg \cdot kg^{-1}$. Fifteen minutes following the i.p.
160 injection, mice were euthanized and tissues harvested.
161

162 *2.8. Hormone and metabolite analysis*

163 Plasma insulin was determined using the Mercodia Ultrasensitive Mouse Insulin ELISA
164 (Mercodia AB, Winston Salem, NC). Liver triglycerides were measured with the Triglycerides -
165 Liquid Reagent Set (Pointe Scientific, Inc., Lincoln Park, MI). Liver glycogen was quantified as
166 previously described [21; 30]. All other metabolites were measured using untargeted metabolomics
167 as detailed below. Tissue metabolite levels were quantified from mice that were fasted 7 hours.

168

169 *2.9. Untargeted metabolomics and ^{13}C-isotope tracing untargeted metabolomics (^{13}C-ITUM)*
170 *pipeline*

171 Extraction and analytical methods were completed as previously described [31-33] with
172 minor modifications. Briefly, lyophilized liver samples (~2 mg) were homogenized in 1000 µL of
173 2:2:1 (v/v/v) acetonitrile (ACN):methanol (MeOH):water and subjected to three (30 second) cycles
174 of vortexing, one minute of flash-freezing in liquid nitrogen, and 10 minutes of sonication at 25°C.
175 Homogenized samples were stored at −20°C for 1 hour and then centrifugated at 15,000 × g for
176 10 minutes at 4 °C. Subsequently, the supernatant was transferred to a fresh tube and dried by
177 SpeedVac overnight. Liver extracts were reconstituted in 100 µL of 1:1 (v/v) ACN:water,
178 sonicated for two (five minute) cycles, vortexed for 1 minute, and then stored at 4°C for one hour.
179 Finally, samples were centrifuged at 15,000 × g at 4 °C for 10 minutes and the supernatants
180 transferred to LC-MS vials. Metabolites were separated using a Thermo Fisher Scientific Vanquish
181 UHPLC system and an Atlantis Premier UPLC BEH Z-HILIC column (186009979, Milford, MA).
182 Mobile Phase A was 90% water with 15 mM ammonium bicarbonate and Mobile Phase B was
183 90% ACN with 15 mM ammonium bicarbonate. The total run time was 10 minutes, flow rate was
184 0.5 mL·min^{-1}, and column chamber temperature was 30°C. Separated metabolites were detected

185 using a Thermo Fisher Scientific QExactive Plus hybrid quadrupole-orbitrap mass spectrometer,
186 fitted with a heated electrospray ionization source operated in negative and positive polarity mode.
187 Two sample types were run to aid in chemical feature identification: 1) a standard mix consisting
188 of authentic standards for all expected analytes and 2) a pooled sample containing only the
189 naturally occurring samples, analyzed via data-dependent analysis (DDA)–tandem mass
190 spectrometry (MS/MS), using IE omics script and R-Studio [34]. Data processing and initial
191 analysis were performed using Thermo Compound Discoverer 3.3. Raw mass spectra were
192 uploaded, background ions were removed, retention times (RT) for detected signals were aligned
193 across samples, and chemical formulas were predicted. Grouped chemical features were profiled
194 to determine compound identity based on: 1) the *m*/*z* predicted from the chemical formula, 2) the
195 RT compared to an authentic external standard, and 3) the MS/MS fragmentation pattern,
196 compared to in-house standards and online databases. For ITUM, putatively identified metabolites
197 were carried forward and subjected to ^{13}C-isotope enrichment with correction for natural
198 abundance. To carry out ^{13}C-isotope tracing, all [^{13}C] mass isotopomers within the isotopic
199 envelope of each identified metabolite were determined based on the diagnostic shift
200 in *m*/*z* ($\Delta m/z$ = 1.0033 Da, natural abundance, 1.11% of all carbon) induced by the presence of ^{13}C-
201 labeled compounds. Raw ion counts for each isotopologue were plotted against RT to generate
202 extracted ion chromatograms, and then the area under the curve for each isotopologue was
203 extracted, summed, and expressed as a percentage of the total pool. After natural abundance
204 correction, the fractional intensities were then graphed as a function of ^{13}C-carbon content,
205 generating mass isotopologue distributions for each detected metabolite. Fractional enrichment
206 reports on the percentage of molecules in a metabolite pool that are ^{13}C-enriched and was
207 calculated by the summation of the relative intensities (% of the total pool) for all ^{13}C mass

208 isotopologues detected. Untargeted metabolomics to determine relative metabolite pools sizes was
209 performed in livers from mice fasted 7 hours to avoid the potential impact of ^{13}C-isotope
210 administration on metabolite abundance.
211
212 *2.10. Targeted analysis of glyoxalase cycle intermediates*
213 Reduced glutathione (GSH), lactoylglutathione (LGSH), and hemithioacetal (HTA) were
214 quantified in liver as previously described [35]. Briefly, samples were prepared in a sulfosalicylic
215 acid solution containing the internal standard, GSH-(Gly-$^{13}C_2$,^{15}N). The protein precipitate was
216 removed via centrifugation and supernatants chromatographed using a Shimadzu LC system
217 equipped with an Atlantis C_{18} column (186001291; Waters, Milford, MA). Multiple reaction
218 monitoring-mass spectrometry (MRM-MS) was performed in positive ion mode using an AB
219 SCIEX 6500+ QTRAP.
220
221 *2.11. Quantitative analysis of arginine and lysine modifications*
222 Lysine lactoylation (lactoyllys), lysine acetylation (acetyllys), methylglyoxal-derived
223 hydroimidazolone 1 (MG-H1), and carboxyethylarginine (CEA) were determined as previously
224 described [35; 36]. Liver protein was precipitated and resuspended in ammonium bicarbonate
225 containing internal standards. Samples were then digested to single amino acids, acidified with
226 heptofluorobutyric acid, chromatographed using a Shimadzu LC system equipped with an Eclipse
227 XDB-C8 column (930990-906; Agilent, Santa Clara, CA), and analyzed by MRM-MS. The post-
228 translational modifications (PTMs) were normalized to Leu to control for digestion [36; 37].
229
230 *2.12. Immunoblotting*

231 Tissue homogenates were prepared as previously detailed [21; 29]. Tissue proteins (15 µg)
232 were separated by electrophoresis on a NuPAGE 4-12% Bis-Tris gel (Invitrogen, Carlsbad, CA,
233 USA) and transferred to a PVDF membrane. Immunoblotting was performed with the primary
234 antibodies and secondary antibodies listed in Supplementary Table 2. The PVDF membranes were
235 treated with a chemiluminescent substrate (Thermo Fisher Scientific, Waltham, MA, USA) and
236 imaged using a ChemiDoc Imaging system and Image Lab software (Bio-Rad, Hercules, CA,
237 USA). Total protein was assessed via BLOT-FastStain (G-Bioscience, St. Louis, MO, USA) and
238 used as the loading control. Densitometry was evaluated using ImageJ software.
239
240 *2.13. Statistical Analysis*
241 GraphPad Prism software (GraphPad Software LLC., San Diego, CA) was used to perform
242 Student's t-test, two-way ANOVAs followed by Tukey's post-hoc tests, and repeated measures
243 ANOVAs followed by Šidák's post-hoc tests as appropriate to detect statistical differences
244 ($p<0.05$). All data are reported as mean ± SEM. Data points greater than two standard deviations
245 from the mean were considered outliers and excluded from analysis.
246
247 **3. RESULTS**
248 *3.1. Elevated glucose partitioning to liver serine by SAAR is linked to improved glucose tolerance*
249 In C57BL/6J mice, 6 weeks of dietary intervention showed a greater gain in body weight,
250 higher adiposity, and similar lean mass in the HF-CTRL compared to LF-CTRL group (Fig. 1A
251 and B). Mice fed a HF-SAAR diet had a lower body weight, decreased fat mass, and increased
252 lean mass percentage relative to both the LF-CTRL and HF-CTRL mice (Fig. 1B). A HF-CTRL
253 diet elevated liver triglycerides compared to mice fed the LF-CTRL diet, while the HF-SAAR diet

254 prevented the increase in liver triglycerides and lowered liver weight (Fig. 1C). Dietary SAAR
255 also lowered liver glycogen and fasting blood glucose (Fig. 1D and E). HF-CTRL mice showed
256 impaired glucose tolerance, but not insulin tolerance, compared to LF-CTRL mice (Fig. 1F and
257 G). Conversely, glucose and insulin tolerance were improved in mice fed the HF-SAAR diet
258 relative to mice fed the LF-CTRL and HF-CTRL diets (Fig. 1F and G). Plasma insulin was
259 significantly reduced in HF-SAAR mice (Fig 1H). This is notable because chronically elevated
260 insulin has been proposed to promoted gain in adiposity and dysregulated glucose control [38-40].
261 To test if the lowered circulating insulin levels in HF-SAAR mice was contributing to the
262 metabolic adaptations to SAAR, a subcutaneous, sustained-release insulin pellet was implanted in
263 HF-SAAR mice to raise insulin. The persistent delivery of exogenous insulin from the
264 subcutaneous pellet over 5 weeks did not impact the glucose and lipid adaptations to SAAR (Suppl.
265 Fig. 1). This suggests that the mechanisms underlying SAAR are independent of circulating insulin
266 concentrations.

267 Untargeted metabolomics revealed that liver cysteine was higher in HF-CTRL compared
268 to LF-CTRL mice (Fig. 2A and 2B). As expected, liver cysteine and taurine were decreased ~5-
269 fold in mice fed the HF-SAAR diet (Fig. 2B). The HF-SAAR diet led to a markedly increased in
270 liver PHGDH (~5-fold) and PSAT1 (~70-fold) protein expression (Fig. 2C). The elevated
271 expression of serine synthesis enzymes was associated with higher liver serine and glycine levels
272 in HF-SAAR relative to both CTRL diet groups (Fig. 2E). The profound increase in PSAT1 protein
273 in the HF-SAAR group made it difficult to resolve differences in PSAT1 in the livers of mice on
274 the LF- and HF-CTRL diets. However, immunoblots performed specifically to compare the LF-
275 CTRL and HF-CTRL groups showed that high-fat feeding decreased liver PSAT1 (Fig. 2D). This
276 was accompanied lower serine concentrations in LF-CTRL versus HF-CTRL mice (Fig. 2E). To

277 test if the increased liver serine and glycine were being sourced from circulating glucose, [U-
278 ^{13}C]glucose was intravenously infused in conscious, unrestrained mice fed a LF-CTRL or a LF-
279 SAAR diet for 6 weeks (Fig. 2F). ^{13}C-labeling of liver serine and glycine was significantly higher
280 in LF-SAAR mice compared to LF-CTRL, with no alterations observed in labeled glucose (Fig.
281 2H). Collectively, our data show that dietary SAAR improves glucose and insulin tolerance, which
282 is associated with increased partitioning of circulating glucose to liver serine synthesis.
283
284 *3.2. Liver PSAT1 is required for SAAR-induced improvements in systemic glucose homeostasis*
285 To assess whether hepatic serine synthesis is essential for the metabolic benefits of dietary
286 SAAR on glucose control, we studied liver-specific PSAT1 KO mice and WT littermates fed a
287 HF-CTRL or -SAAR diet (Fig. 3A). The HF-SAAR diet prevented a gain in body weight and
288 adiposity in both genotypes (Fig. 3B and C). When fed a HF-CTRL diet, WT and liver PSAT1 KO
289 mice showed similar glucose tolerance (Fig. 3D). This was expected given that high-fat feeding
290 lowers liver PSAT1 in WT mice (Fig. 2D), a phenotype closely resembling liver PSAT1 KO mice.
291 On a HF-SAAR diet, liver-specific PSAT1 KO mice showed a greater excursion of glucose at the
292 15- and 30-minute time points during the glucose tolerance test compared to WT mice, although
293 the area under the curve was comparable between genotypes (Fig. 3D). Loss of hepatic PSAT1 in
294 mice fed HF-CTRL diet delayed the normalization of circulating glucose during an insulin
295 tolerance test relative to WT littermates (Fig. 3E). Six weeks of HF-SAAR feeding improved
296 insulin tolerance similarly in WT and KO mice compared to HF-CTRL groups (Fig. 3E).
297 Concordant with the C57BL/6J findings (Fig. 1), HF-SAAR feeding lowered plasma insulin levels
298 relative to mice fed a HF-CTRL diet in both genotypes (Fig. 3F). Fifteen minutes after an insulin
299 injection, the liver p-Akt-to-Akt ratio was higher in both genotypes fed the HF-SAAR diet (Fig.

300 3G). This suggests liver insulin signaling was enhanced similarly in WT and KO mice following
301 SAAR. Dietary SAAR lowered liver glycogen in WT and liver PSAT1 KO mice (Fig. 3H).
302 However, this was independent of changes key enzymes regulating glycogen synthesis and
303 breakdown. Specifically, total protein and the phospho-to-total protein ratio for glycogen synthase
304 (GS) and glycogen phosphorylase (PYGL) were similar between groups (Fig. 3I). Together, these
305 data indicate that liver PSAT1 is necessary for dietary SAAR to improve whole-body glucose
306 tolerance.
307
308 *3.3. Increased glucose partitioning to serine following SAAR is abolished by loss of hepatic PSAT1*
309 Next, we aimed to further connect the attenuated improvement in glucose tolerance
310 observed in liver PSAT1 KO mice fed a HF-SAAR diet to inability of hepatocytes to synthesize
311 serine from glucose (Fig. 4A). The HF-SAAR diet elevated serine and glycine synthesis enzymes,
312 PHGDH, PSAT1 (WT mice only), and serine hydroxymethyltransferase 2 (SHMT2), in the livers
313 of mice (Fig. 4B). Under post-absorptive conditions, liver glucose, serine, and glycine were
314 comparable between WT and KO mice fed a HF-CTRL diet (Fig. 4C). Dietary SAAR lowered
315 liver glucose in WT, but not liver PSAT1 KO mice (Fig. 4C). Liver serine and glycine were higher
316 in WT mice fed a HF-SAAR diet compared to WT mice on a HF-CTRL diet (Fig. 4C); however,
317 the increase in liver serine and glycine by SAAR was blunted in liver PSAT1 KO mice (Fig. 4C).
318 Consistent with these metabolite levels, a HF-SAAR diet prompted a rise in the ^{13}C-labeling of
319 liver serine and glycine in WT mice intravenously infused with [U-^{13}C]glucose (Fig. 4D). Loss of
320 liver PSAT1 attenuated the increased in serine and glycine ^{13}C-labeling by SAAR (Fig. 4D). These
321 data imply that the improved glucose tolerance by dietary SAAR is associated with enhanced
322 partitioning of circulating glucose to liver serine synthesis.

323

324 *3.4. Serine sourced from glucose following SAAR is preferentially fated to glutathione*

325 Serine is a precursor for cysteine synthesis via transsulfuration and donates a one-carbon
326 units to support methionine regeneration within the methionine cycle [41]. Given this, one could
327 speculate that the elevated diversion of glucose to serine is an adaptive response to prevent
328 limitations in SAA availability that may arise from dietary SAAR. To further test this hypothesis,
329 liver proteins, metabolite concentrations, and metabolite labeling from [U-^{13}C]glucose and [U-
330 ^{13}C]serine administration were determined (Fig. 5). Regardless of diet, loss of hepatic PSAT1 did
331 not impact proteins involved in transsulfuration or cysteine catabolism (Fig. 5A and 5B). Dietary
332 SAAR increased cystathionine γ-lyase (CSE; involved in cysteine production), decreased cysteine
333 dioxygenase 1 (CDO1; involved in cysteine catabolism to taurine), and elevated GSH synthesis
334 enzymes, glutamate-cysteine ligase catalytic subunit (GCLC) and glutathione synthetase (GSS),
335 in both genotypes (Fig. 5A and 5B). SAAs and related metabolites were comparable between WT
336 and liver PSAT1 KO mice fed a HF-CTRL diet (Fig. 5C). The HF-SAAR diet decreased liver
337 cysteine, taurine, GSH, and oxidized glutathione (GSSG) in both genotypes compared to their
338 counterparts fed the HF-CTRL diet (Fig. 5C). Consistent with metabolite levels, ^{13}C-labeling of
339 liver SAA and related metabolites following a 30-minute [U-^{13}C]glucose infusion was similar
340 between WT and Liver PSAT1 KO mice on a HF-CTRL diet (Fig. 5D). HF-SAAR feeding
341 increased ^{13}C-labeling from glucose in liver methionine in both WT and liver PSAT1 KO mice
342 (Fig. 5D). Fractional enrichment in liver cysteine was not detectable due to the low cysteine pool
343 in mice fed a HF-SAAR diet; however, downstream fates of cysteine were measured. The [U-
344 ^{13}C]glucose infusion showed lower ^{13}C-taurine, and increased ^{13}C-GSH and ^{13}C-GSSG in the
345 livers of both WT and KO mice fed the HF-SAAR diet relative to the HF-CTRL mice (Fig. 5D),

346 with the SAAR-mediated increase in GSH and GSSG ^{13}C-labeling from [U-^{13}C]glucose being
347 blunted in liver PSAT1 KO mice compared to their WT littermates (Fig. 5D). To more directly
348 assess the impact of dietary SAAR on serine fate, [U-^{13}C]serine was administered to WT mice fed
349 a HF-CTRL or a HF-SAAR diet for 6 weeks (Fig. 5E). ^{13}C-labeling was increased in liver
350 methionine, taurine, GSH, and GSSG in the HF-SAAR mice compared to the HF-CTRL (Fig. 5E).
351 The rise in ^{13}C-labeling was particularly pronounced for GSH (~12-fold) and GSSG (~37-fold)
352 (Fig. 5E). Together, these results suggest that serine synthesized *de novo* from glucose is important
353 for supporting GSH provision during SAAR.
354
355 *3.5. SAAR reduces glyoxalase cycle intermediates and associated protein PTMs*
356 To further explore the potential connectivity between serine synthesis and GSH
357 availability, we assessed markers of glyoxalase cycle metabolism (Fig. 6A). GSH can be used to
358 generate LGSH in the glyoxalase cycle and recent work identified LGSH-derived lysine
359 lactoylation inhibits PHGDH [42]. Liver glyoxalase cycle enzymes, glyoxalase 1 (GLO1) and
360 hydroxyacylglutathione hydrolase (GLO2), were comparable between genotypes on both diets
361 (Fig. 6B). However, SAAR decreased liver GLO1 protein (Fig. 6B). Consistent with data from our
362 untargeted metabolomic approaches (Fig. 5C), targeted quantification showed lower liver GSH in
363 WT and KO mice fed a HF-SAAR diet compared to the HF-CTRL diet (Fig. 6C). Dietary SAAR
364 also decreased liver LGSH and HTA in both genotypes (Fig 6C). Liver lactate was lower in liver
365 PSAT1 KO mice relative to WT mice fed HF-CTRL (Fig. 6C). SAAR decreased liver lactate in
366 WT, but not liver PSAT1 KO mice (Fig. 6C). PTMs derived from glyoxalase cycle metabolites
367 were broadly suppressed by SAAR. Specifically, lysine lactoylation was decreased in HF-SAAR
368 WT mice compared to WT HF-CTRL (Fig. 6D). In contrast, lysine lactoylation was comparable

369 between liver PSAT1 KO mice fed the HF-CTRL and -SAAR diets (Fig. 6D). Methylglyoxal
370 (MGO)-derived modifications, MG-H1 and CEA, were significantly lower in HF-SAAR- versus
371 HF-CTRL-fed mice regardless of genotype (Fig. 6D). Global lysine acetylation was not changed
372 by diet or genotype (Fig. 6D). Overall, SAAR reduces glyoxalase-cycle intermediates and the
373 protein modifications they support.
374
375 *3.6. SAAR diverts glucose toward asparagine synthesis*
376 Given that loss of hepatic PSAT1 blunted, but did not completely abolish the improvement
377 in glucose tolerance by SAAR, we further examined how SAAR could be influencing glucose
378 metabolism in the liver. On a HF-CTRL diet, liver TCA cycle, anaplerotic, and cataplerotic
379 metabolites were mostly comparable between WT and KO mice (Fig. 7A and B). SAAR increased
380 pyruvate, decreased malate (WT mice only), and elevated aspartate (Fig. 7B). [U-^{13}C]glucose
381 tracing showed lower ^{13}C-pyruvate, increased ^{13}C-aspartate, and significantly elevated ^{13}C-
382 asparagine (~370-fold) labeling in WT and KO mice on the HF-SAAR diet compared to the HF-
383 CTRL diet (Fig. 7C). Interestingly, SAAR lowered the ^{13}C-labeling of liver succinate in WT mice
384 (Fig. 7C). This decreased ^{13}C-labeling of liver TCA cycle intermediates was more pronounced in
385 PSAT1 KO mice on a HF-SAAR diet as indicated by lower ^{13}C-citrate, ^{13}C-succinate, and ^{13}C-
386 malate (Fig. 7C). Next, we assessed three isotopologue ratios to provide indices of nutrient flux
387 [43-48]. Livers of WT mice fed the HF-SAAR diet had a higher citrate M+3-to-pyruvate M+3
388 ratio relative to WT mice fed a HF-CTRL and KO mice fed a HF-SAAR diet (Fig. 7D). This
389 suggests that TCA cycle anaplerosis via pyruvate carboxylase (PC) was stimulated by SAAR. The
390 aspartate M+3-to-succinate M+3 and aspartate M+3-to-citrate M+3 ratios were elevated in HF-
391 SAAR mice compared to their HF-CTRL counterparts (Fig. 7D). The increase in these two ratios

392 suggest a preferential partitioning of pyruvate to aspartate compared to flux through the TCA
393 cycle. Consistent with the metabolite and ^{13}C-isotope tracing data, liver asparagine synthetase
394 (ASNS) protein was ~25-fold higher in mice fed a HF-SAAR diet compared to those receiving the
395 HF-CTRL diet (Fig. 7E). Most TCA cycle proteins tested were not altered by diet or genotype
396 (Fig. 7E). The cataplerotic enzyme, mitochondrial glutamic-oxaloacetic transaminase (GOT2),
397 was increased in PSAT1 KO mice fed a HF-SAAR diet compared to both their WT littermates and
398 KO mice fed HF-CTRL (Fig. 7E). These results indicate that SAAR shifts the fate of glucose, via
399 the TCA cycle anaplerosis, towards liver asparagine synthesis.
400
401 *3.7. SAAR prevents liver lipid accumulation independently of hepatic PSAT1*
402 In addition to glucose control, we investigated the role of hepatic PSAT1 action in liver
403 lipid adaptations to dietary SAAR. After 6 weeks of diet, liver triglycerides were lower in WT
404 mice fed a HF-SAAR diet compared to WT mice on the HF-CTRL diet (Fig. 8A). This dietary
405 effect was not observed in liver PSAT1 KO mice (Fig. 8A). The expression of liver *de novo*
406 lipogenesis enzymes, ATP-citrate lyase (ACLY) and stearoyl-CoA desaturase 1 (SCD1), were
407 suppressed with HF-SAAR feeding in both genotypes (Fig. 8B and D). SAAR decreased FASN
408 protein in WT mice only (Fig. 8B and D). Given that hepatic triglyceride concentrations may also
409 be impacted by changes in lipid catabolism, we next examined mitochondrial respiratory proteins
410 as a marker of potential changes in mitochondrial oxidative metabolism in response to SAAR. As
411 we previously observed [21], SAAR increased liver mitochondrial respiratory proteins (Fig. 8C
412 and D). Specifically, complex I (NADH dehydrogenase (ubiquinone) iron-sulfur protein 4;
413 NDUFS4) and complex V (ATP synthase F1 subunit alpha; ATP5A) were higher in WT mice fed
414 HF-SAAR compared to WT mice fed the HF-CTRL diet. (Fig. 8C and D). Complex IV

415 (mitochondrial encoded cytochrome c oxidase subunit II; MTCO2) protein was elevated in PSAT1
416 KO mice on the HF-SAAR diet versus KO mice fed the HF-CTRL diet (Fig. 8C and D). An
417 additional mechanism through which SAAR may lower liver triglycerides is the formation of
418 acylglycines (Fig. 8E). Protein expression of liver glycine N-acyltransferase (GLYAT), which
419 catalyzes the conjugation of acyl-CoA to glycine, was similar between groups (Fig. 8F). However,
420 HF-SAAR raised the levels of short-chain acylglycines (acetylglycine, isobutyrylglycine, and
421 isovalerylglycine) in the liver (Fig. 8G).

422 To further test if hepatic PSAT1 action was required for SAAR to lower liver triglycerides,
423 mice were fed the HF-SAAR diet for 20 weeks. Both WT and KO mice fed the HF-SAAR diet
424 had lower body weight, fat mass, and liver triglycerides compared to mice on the HF-CTRL diet
425 (Fig. 8H-J). This suggest that hepatic PSAT1 is not needed, particularly with increasing duration,
426 for SAAR to promotes a decline in liver triglycerides.

427

428 **4. DISCUSSION**

429 Dietary SAAR prevents obesity, dysregulated glucose control, and liver steatosis [1].
430 Analysis of changes at the level of the transcriptome has identified that the liver is particularly
431 responsive to SAAR [1]. These changes include an increased expression of liver *de novo* serine
432 synthesis pathway enzyme, PSAT1, which is among the most reproducible responses to dietary
433 SAAR [2; 9; 10; 15-23]. Given the interconnectedness of *de novo* serine synthesis with glycolysis
434 and gluconeogenesis pathways, this study tested the hypothesis that hepatic PSAT1 is needed for
435 the liver glucose and lipid adaptations to SAAR. The pertinent findings of this study are: 1)
436 enhanced hepatic *de novo* serine synthesis is required for SAAR to improve glucose tolerance, 2)
437 concurrent with transcriptional activation, a serine synthesis-GSH-lysine lactoylation feedback

438 loop may underlie the increased hepatic serine synthesis in response to SAAR, and 3) hepatic
439 serine synthesis is not necessary for the SAAR-mediated decline in adiposity and liver
440 triglycerides.
441
442 *4.1. Role of hepatic PSAT1 in glucose adaptations to SAAR*
443 Consistent with previous studies using rodents [2-7], we found that dietary SAAR
444 enhances glucose tolerance. Untargeted metabolomics showed this whole-body glucose phenotype
445 was associated with increased liver serine. Exogenous serine supplementation can [49], but does
446 not always [50], improve glucose tolerance. Thus, the SAAR-mediated increase in serine may
447 actively promote glucose tolerance via one or more downstream functions [51]. Our ^{13}C-isotope
448 tracing experiments showed elevated partitioning of circulating glucose to hepatic serine following
449 SAAR. Moreover, loss of hepatic PSAT1 impaired glucose tolerance in mice fed the SAAR diet
450 and abolished the increase in liver serine sourced from circulating glucose without completely
451 preventing the rise in liver serine levels. These results suggest that a higher rate of hepatic glucose
452 disposal and the diversion of glucose to the synthesis of serine is, in part, responsible for the
453 SAAR-mediated adaptations in whole-body glucose control.
454 PSAT1 overexpression in mice enhances both glucose and insulin tolerance [26]. In the
455 experiments presented here, we found that the heightened insulin tolerance following SAAR was
456 not impacted by the loss of hepatic PSAT1. Prior work has reported that the enhanced insulin
457 action in response to PSAT1 overexpression is mediated by decreased expression of tribbles
458 homolog 3 (TRB3), which is a pseudokinase that inhibits insulin signaling by binding to Akt and
459 impairing its activation by phosphorylation [26]. Our studies showed the phosphorylation of liver
460 Akt was elevated similarly in both WT and liver PSAT1 KO mice. Together, these data suggest

461 the elevated liver PSAT1 increases glucose tolerance independent of insulin action. However,
462 future work should assess the role of liver PSAT1 on liver insulin action during hyperinsulinemic-
463 euglycemic clamps combined with isotope tracers. These conditions would allow for assessing
464 liver-specific insulin sensitivity under euglycemic conditions so that the impact of SAAR on
465 extrahepatic glucose flux and concentrations do not mask alterations at the liver.
466
467 *4.2. Potential mechanisms promoting increased hepatic de novo serine synthesis from glucose*
468 Work by independent groups indicate that SAAs negatively regulate serine synthesis.
469 Cysteine suppresses the expression of PHGDH by decreasing mRNA stability [52]. In addition to
470 post-transcriptional regulation, mechanisms at the level of transcription may also contribute to the
471 enhanced serine synthesis by SAAR. Deletion of the transcription factor, nuclear factor erythroid
472 2-related factor 2 (NRF2), in the livers of mice blunted but did not abolish the increase in PSAT1
473 mRNA [16]. These mechanisms of action are consistent with the elevated liver PHGDH and
474 PSAT1 mRNA and protein in response to SAAR. Serine is a precursor for cysteine, which is
475 generated via transsulfuration wherein the sulfur from methionine is transferred to serine [41]. It
476 may be that increased cysteine impedes the synthesis of its precursor, serine, to control SAA levels.
477 Conversely, when cysteine is low, serine synthesis is stimulated to promote SAA availability.
478 Ultimately, these findings suggest that SAAR-mediated increase in glucose tolerance is the result
479 of liver responses to maintain SAA homeostasis via serine synthesis.
480 A prominent fate of methionine and cysteine, particularly under conditions of low SAA
481 levels, is the synthesis of GSH [53-56]. Aligning with prior studies [23], we observed liver GSH
482 was decreased by SAAR. However, our [U-^{13}C]glucose and [U-^{13}C]serine isotope tracing
483 experiments showed that ^{13}C-labeling of liver GSH and GSSG was elevated in mice fed the SAAR

484 diet. While the [U-^{13}C]serine tracing showed SAAR increased labeling of other fates of cysteine
485 such as taurine, loss of hepatic PSAT1 uniquely attenuated the increased liver ^{13}C-GSH and ^{13}C-
486 GSSG from [U-^{13}C]glucose. These results indicate that serine synthesized *de novo* from glucose
487 is important to support GSH provision (via cysteine) during SAAR.

488 Beyond its antioxidant properties, GSH is a metabolite within the glyoxalase cycle. This
489 highly conserved metabolic cycle comprised of two enzymes, GLO1 and GLO2, uses GSH to
490 catabolize MGO to lactate through the intermediate, LGSH [57]. LGSH is an acyl-donor in a non-
491 enzymatic reaction with free lysine residues, yielding the PTM, lysine lactoylation [35; 58]. This
492 is notable because PHGDH and PSAT1 are heavily lactoylated and LGSH inhibits PHGDH
493 activity [35; 42]. Our results showed that SAAR lowered liver LGSH and lysine lactoylation.
494 Together, our data and the work of others suggest that SAAR may increase serine synthesis by
495 preventing the inhibition of PHGDH and/or PSAT1 by LGSH-derived lysine lactoylation.
496 Consistent with GSH regulating serine synthesis via post-translational mechanisms, the
497 pharmacologic inhibition of GSH synthesis using buthionine sulfoximine increased liver serine
498 without altering NRF2 or PHGDH expression [22]. While it remains to be fully tested, SAAR may
499 promote glucose tolerance through a hepatic serine synthesis-GSH-lysine lactoylation feedback
500 loop in which low SAA decreases liver GSH, lowers lysine lactoylation, and thereby prevents
501 inhibition of *de novo* serine synthesis from glucose.

502

503 *4.3. SAAR shifts the fate of glucose towards liver asparagine*

504 In addition to *de novo* serine synthesis, this study demonstrates that SAAR stimulates
505 glucose partitioning towards asparagine synthesis. Liver asparagine concentration was similar
506 between mice fed the HF-CTRL and SAAR diets. However, ^{13}C-labeling of liver asparagine from

507 [U-^{13}C]glucose increased markedly by ~370-fold in SAAR-fed mice. We also assessed indices of
508 nutrient flux [43-48]. Isotopologue ratios from our [U-^{13}C]glucose tracing experiments are
509 consistent with SAAR increasing TCA cycle anaplerosis through PC (i.e., the generation of OAA
510 from pyruvate) and the resulting OAA being preferentially directed to asparagine rather than flux
511 through the TCA cycle. In agreement with this, Xin et al.[59] show that SAAR increases liver
512 TCA cycle anaplerosis as evidenced by higher enrichment of TCA cycle metabolites following the
513 administration of [U-^{13}C]glucose and [U-^{13}C,^{15}N]glutamine. Herein, we show the SAAR-induced
514 shift in glucose and TCA cycle intermediates to asparagine was associated with a ~25-fold increase
515 in liver ASNS, which generates asparagine from aspartate. SAAR did not alter the expression of
516 other anaplerotic and cataplerotic enzymes (i.e., PC, MDH2, PCCA, and GOT2) linked to
517 asparagine synthesis. Interestingly, these aforementioned enzymes have been reported to be
518 modified by lysine lactoylation [35]. Thus, further research is warranted to determine if the SAAR-
519 driven reduction in lactoylation prevents the inhibition of these enzymes and favors the diversion
520 of glucose to asparagine. Future studies should also test whether the stimulation glucose
521 partitioning to asparagine is an additional means through which SAAR increases glucose tolerance.
522 The shift in glucose fate to asparagine during SAAR could be an additional means of
523 enhancing serine availability. Intracellular asparagine exchanges with extracellular serine to
524 promote serine uptake [60]. Liver PSAT1 KO mice receiving a HF-SAAR diet showed higher liver
525 serine levels compared to KO mice fed a HF-CTRL diet. This was accompanied by a trend towards
526 greater ^{13}C-labeling of liver serine [U-^{13}C]glucose in KO mice fed a HF-SAAR diet compared to
527 KO mice fed a HF-CTRL diet. To further explore if the liver was acquiring this serine from
528 extrahepatic sources, we administered [U-^{13}C]serine to mice. Liver ^{13}C-serine labeling was similar
529 between mice fed a HF-CTRL and HF-SAAR diet. Given that the liver serine pool size is larger

530 in mice fed a HF-SAAR diet, a greater amount of exogenous ^{13}C-serine would need to be taken up
531 by the liver to achieve a similar proportion of ^{13}C-serine labeling in livers of mice fed a HF-SAAR
532 diet. Thus, our data aligns with the hypothesis that SAAR increases asparagine synthesis from
533 glucose to promote liver serine uptake.
534
535 *4.4. Role of hepatic PSAT1 in lipid adaptations to SAAR*
536 Our findings agree with prior studies reporting that SAAR lowers adiposity and liver
537 triglycerides [2; 5; 9; 18; 21; 59]. In the current study, the decline in liver triglycerides following
538 SAAR was associated with decreased *de novo* lipogenesis enzymes (ACLY, FASN, and SCD-1).
539 There was a modest increase in mitochondrial respiratory chain proteins (complexes I, IV, and V)
540 in response to SAAR. These results are consistent with our prior work showing dietary SAAR
541 increases the expression of select mitochondrial proteins without enhancing mitochondrial
542 respiration [21]. While terminal oxidation may not be enhanced by SAAR [21], other means of
543 lipid disposal could contribute to lower triglycerides. Studies using ^{14}C-palmitate in liver
544 homogenates have determined that SAAR increases liver β-oxidation [61]. We identified short-
545 chain acylglycines (acetylglycine, isobutyrylglycine, and isovalerylglycine) were increased. These
546 acylglycines are generated in the mitochondria by conjugating acyl-CoAs to glycine in a reaction
547 mediated by GLYAT [62]. Thus, the SAAR-mediated rise in glycine may facilitate acylglycine
548 synthesis and, consequently, promote the disposal of fatty acids during SAAR. Importantly, SAAR
549 elicited the molecular responses in lipid metabolism and lowered liver triglycerides similarly in
550 WT and PSAT1 KO mice. Overall, the prevailing signature under SAAR is a coordinated decrease
551 in *de novo* lipogenesis and stimulation of acyl-CoA disposal that is independent of PSAT1 action.
552

In summary, hepatic PSAT1 is necessary for adaptations to SAAR involving serine synthesis that allow improvements in glucose tolerance to be fully realized. In contrast, PSAT1 is dispensable for the adaptations in lipid accretion and disposal pathways that contribute to the SAAR-mediated decline in liver lipids. Thus, the serine synthesis pathway is critical to the glucose, but not lipid, adaptations to SAAR. These studies provide a mechanistic foundation for how SAAR impacts the liver to prevent dysregulated glucose control.

ACKNOWLEDGEMENTS

The authors acknowledge the technical assistance provided by Ruth Pfeiffer. Figure schematics were created using BioRender.com.

CRediT AUTHORSHIP CONTRIBUTION STATEMENT

A.F.O.: Writing – original draft, Visualization, Validation, Methodology, Investigation, Formal analysis, Data curation, Conceptualization, and Project administration C.V., F.I.R., K.M.A., A.M.P., and A.B.N.: Investigation, and Writing - Review & Editing; P.A.C., and J.J.G.: Methodology, Resources, and Writing - Review & Editing; S.C.H.: Resources, and Writing - Review & Editing; C.C.H.: Writing – review & editing, Visualization, Validation, Supervision, Resources, Methodology, Investigation, Funding acquisition, Dara curation, Conceptualization, and Project administration.

FUNDING SOURCES

The National Institutes of Health Grants DK136772 (C.C.H.), DK091538 (P.A.C.), AG069781 (P.A.C.), DK133196 (J.J.G.) supported this research. A.F.O. was supported by the National Institutes of Health Ruth L. Kirschstein National Research Service Award T32 DK007293.

DECLARATION OF COMPETING INTEREST

The authors declare that they have no known competing financial interests or personal relationships that could have appeared to influence the work reported in this paper.

REFERENCES

[1] Fang, H., Stone, K.P., Wanders, D., Forney, L.A., Gettys, T.W., 2022. The Origins, Evolution, and Future of Dietary Methionine Restriction. Annu Rev Nutr 42:201-226.

[2] Forney, L.A., Wanders, D., Stone, K.P., Pierse, A., Gettys, T.W., 2017. Concentration-dependent linkage of dietary methionine restriction to the components of its metabolic phenotype. Obesity (Silver Spring) 25(4):730-738.

[3] Malloy, V.L., Krajcik, R.A., Bailey, S.J., Hristopoulos, G., Plummer, J.D., Orentreich, N., 2006. Methionine restriction decreases visceral fat mass and preserves insulin action in aging male Fischer 344 rats independent of energy restriction. Aging Cell 5(4):305-314.

[4] Thyne, K.M., Salmon, A.B., 2022. Metabolic benefits of methionine restriction in adult mice do not require functional methionine sulfoxide reductase A (MsrA). Sci Rep 12(1):5073.

[5] Lees, E.K., Banks, R., Cook, C., Hill, S., Morrice, N., Grant, L., et al., 2017. Direct comparison of methionine restriction with leucine restriction on the metabolic health of C57BL/6J mice. Sci Rep 7(1):9977.

[6] Lees, E.K., Krol, E., Grant, L., Shearer, K., Wyse, C., Moncur, E., et al., 2014. Methionine restriction restores a younger metabolic phenotype in adult mice with alterations in fibroblast growth factor 21. Aging Cell 13(5):817-827.

[7] Ables, G.P., Perrone, C.E., Orentreich, D., Orentreich, N., 2012. Methionine-restricted C57BL/6J mice are resistant to diet-induced obesity and insulin resistance but have low bone density. PLoS One 7(12):e51357.

[8] Wanders, D., Burk, D.H., Cortez, C.C., Van, N.T., Stone, K.P., Baker, M., et al., 2015. UCP1 is an essential mediator of the effects of methionine restriction on energy balance but not insulin sensitivity. FASEB J 29(6):2603-2615.

[9] Wanders, D., Forney, L.A., Stone, K.P., Burk, D.H., Pierse, A., Gettys, T.W., 2017. FGF21 Mediates the Thermogenic and Insulin-Sensitizing Effects of Dietary Methionine Restriction but Not Its Effects on Hepatic Lipid Metabolism. Diabetes 66(4):858-867.

[10] Wanders, D., Stone, K.P., Forney, L.A., Cortez, C.C., Dille, K.N., Simon, J., et al., 2016. Role of GCN2-Independent Signaling Through a Noncanonical PERK/NRF2 Pathway in the Physiological Responses to Dietary Methionine Restriction. Diabetes 65(6):1499-1510.

[11] Stone, K.P., Wanders, D., Orgeron, M., Cortez, C.C., Gettys, T.W., 2014. Mechanisms of increased in vivo insulin sensitivity by dietary methionine restriction in mice. Diabetes 63(11):3721-3733.
[12] Plaisance, E.P., Greenway, F.L., Boudreau, A., Hill, K.L., Johnson, W.D., Krajcik, R.A., et al., 2011. Dietary methionine restriction increases fat oxidation in obese adults with metabolic syndrome. J Clin Endocrinol Metab 96(5):E836-840.
[13] Olsen, T., Stolt, E., Ovrebo, B., Elshorbagy, A., Tore, E.C., Lee-Odegard, S., et al., 2024. Dietary sulfur amino acid restriction in humans with overweight and obesity: a translational randomized controlled trial. J Transl Med 22(1):40.
[14] Richie, J.P., Jr., Sinha, R., Dong, Z., Nichenametla, S.N., Ables, G.P., Ciccarella, A., et al., 2023. Dietary Methionine and Total Sulfur Amino Acid Restriction in Healthy Adults. J Nutr Health Aging 27(2):111-123.
[15] Fang, H., Stone, K.P., Ghosh, S., Forney, L.A., Gettys, T.W., 2021. The Role of Reduced Methionine in Mediating the Metabolic Responses to Protein Restriction Using Different Sources of Protein. Nutrients 13(8).
[16] Fang, H., Stone, K.P., Ghosh, S., Forney, L.A., Sims, L.C., Vincik, L., et al., 2021. Hepatic Nfe2l2 Is Not an Essential Mediator of the Metabolic Phenotype Produced by Dietary Methionine Restriction. Nutrients 13(6).
[17] Fang, H., Stone, K.P., Forney, L.A., Sims, L.C., Gutierrez, G.C., Ghosh, S., et al., 2021. Implementation of dietary methionine restriction using casein after selective, oxidative deletion of methionine. iScience 24(5):102470.
[18] Stone, K.P., Ghosh, S., Kovalik, J.P., Orgeron, M., Wanders, D., Sims, L.C., et al., 2021. The acute transcriptional responses to dietary methionine restriction are triggered by inhibition of ternary complex formation and linked to Erk1/2, mTOR, and ATF4. Sci Rep 11(1):3765.
[19] Forney, L.A., Fang, H., Sims, L.C., Stone, K.P., Vincik, L.Y., Vick, A.M., et al., 2020. Dietary Methionine Restriction Signals to the Brain Through Fibroblast Growth Factor 21 to Regulate Energy Balance and Remodeling of Adipose Tissue. Obesity (Silver Spring) 28(10):1912-1921.
[20] Ghosh, S., Forney, L.A., Wanders, D., Stone, K.P., Gettys, T.W., 2017. An integrative analysis of tissue-specific transcriptomic and metabolomic responses to short-term dietary methionine restriction in mice. PLoS One 12(5):e0177513.
[21] Rome, F.I., Hughey, C.C., 2022. Disrupted liver oxidative metabolism in glycine N-methyltransferase-deficient mice is mitigated by dietary methionine restriction. Mol Metab 58:101452.
[22] Ommi, N.B., Mattocks, D.A.L., Kalecky, K., Bottiglieri, T., Nichenametla, S.N., 2025. Pharmacological recapitulation of the lean phenotype induced by the lifespan-extending sulfur amino acid-restricted diet. Aging (Albany NY) 17(4):960-981.
[23] Nichenametla, S.N., Mattocks, D.A.L., Cooke, D., Midya, V., Malloy, V.L., Mansilla, W., et al., 2022. Cysteine restriction-specific effects of sulfur amino acid restriction on lipid metabolism. Aging Cell 21(12):e13739.
[24] Kalhan, S.C., Hanson, R.W., 2012. Resurgence of serine: an often neglected but indispensable amino Acid. J Biol Chem 287(24):19786-19791.
[25] Hamano, M., Esaki, K., Moriyasu, K., Yasuda, T., Mohri, S., Tashiro, K., et al., 2021. Hepatocyte-Specific Phgdh-Deficient Mice Culminate in Mild Obesity, Insulin Resistance, and Enhanced Vulnerability to Protein Starvation. Nutrients 13(10).

[26] Yu, J., Xiao, F., Guo, Y., Deng, J., Liu, B., Zhang, Q., et al., 2015. Hepatic Phosphoserine Aminotransferase 1 Regulates Insulin Sensitivity in Mice via Tribbles Homolog 3. Diabetes 64(5):1591-1602.

[27] Sim, W.C., Lee, W., Sim, H., Lee, K.Y., Jung, S.H., Choi, Y.J., et al., 2020. Downregulation of PHGDH expression and hepatic serine level contribute to the development of fatty liver disease. Metabolism 102:154000.

[28] Raines, L.N., Zhao, H., Wang, Y., Chen, H.-Y., Gallart-Ayala, H., Hsueh, P.-C., et al., 2022. PERK is a critical metabolic hub for immunosuppressive function in macrophages. Nature immunology 23(3):431-445.

[29] Rome, F.I., Shobert, G.L., Voigt, W.C., Stagg, D.B., Puchalska, P., Burgess, S.C., et al., 2023. Loss of hepatic phosphoenolpyruvate carboxykinase 1 dysregulates metabolic responses to acute exercise but enhances adaptations to exercise training in mice. Am J Physiol Endocrinol Metab 324(1):E9-E23.

[30] Chan, T.M., Exton, J.H., 1976. A rapid method for the determination of glycogen content and radioactivity in small quantities of tissue or isolated hepatocytes. Analytical biochemistry 71(1):96-105.

[31] Puchalska, P., Crawford, P.A., 2019. Application of stable isotope labels for metabolomics in studies in fatty liver disease. Metabolomics: Methods and Protocols. Springer, p. 259-272.

[32] Nelson, A.B., Reese, L.E., Rono, E., Queathem, E.D., Qiu, Y., McCluskey, B.M., et al., 2025. Deciphering Colorectal Cancer–Hepatocyte Interactions: A Multiomics Platform for Interrogation of Metabolic Crosstalk in the Liver–Tumor Microenvironment. International journal of molecular sciences 26(5):1976.

[33] Queathem, E.D., Moazzami, Z., Stagg, D.B., Nelson, A.B., Fulghum, K., Hayir, A., et al., 2025. Ketogenesis supports hepatic polyunsaturated fatty acid homeostasis via fatty acid elongation. Science Advances 11(5):eads0535.

[34] Koelmel, J.P., Kroeger, N.M., Gill, E.L., Ulmer, C.Z., Bowden, J.A., Patterson, R.E., et al., 2017. Expanding lipidome coverage using LC-MS/MS data-dependent acquisition with automated exclusion list generation. Journal of the American Society for Mass Spectrometry 28(5):908-917.

[35] Gaffney, D.O., Jennings, E.Q., Anderson, C.C., Marentette, J.O., Shi, T., Schou Oxvig, A.M., et al., 2020. Non-enzymatic Lysine Lactoylation of Glycolytic Enzymes. Cell Chem Biol 27(2):206-213 e206.

[36] Galligan, J.J., Wepy, J.A., Streeter, M.D., Kingsley, P.J., Mitchener, M.M., Wauchope, O.R., et al., 2018. Methylglyoxal-derived posttranslational arginine modifications are abundant histone marks. Proc Natl Acad Sci U S A 115(37):9228-9233.

[37] Galligan, J.J., Kingsley, P.J., Wauchope, O.R., Mitchener, M.M., Camarillo, J.M., Wepy, J.A., et al., 2017. Quantitative Analysis and Discovery of Lysine and Arginine Modifications. Anal Chem 89(2):1299-1306.

[38] Mehran, A.E., Templeman, N.M., Brigidi, G.S., Lim, G.E., Chu, K.Y., Hu, X., et al., 2012. Hyperinsulinemia drives diet-induced obesity independently of brain insulin production. Cell Metab 16(6):723-737.

[39] Thomas, D.D., Corkey, B.E., Istfan, N.W., Apovian, C.M., 2019. Hyperinsulinemia: An Early Indicator of Metabolic Dysfunction. J Endocr Soc 3(9):1727-1747.

[40] Wiebe, N., Ye, F., Crumley, E.T., Bello, A., Stenvinkel, P., Tonelli, M., 2021. Temporal Associations Among Body Mass Index, Fasting Insulin, and Systemic Inflammation: A Systematic Review and Meta-analysis. JAMA Network Open 4(3):e211263-e211263.
[41] Werge, M.P., McCann, A., Galsgaard, E.D., Holst, D., Bugge, A., Albrechtsen, N.J.W., et al., 2021. The Role of the Transsulfuration Pathway in Non-Alcoholic Fatty Liver Disease. J Clin Med 10(5).
[42] Trujillo, M.N., Jennings, E.Q., Farrera, D.O., Kitamura, N., Anderson, C.C., Gehrke, S., et al., 2025. Glyoxalase 2 Coordinates de Novo Serine Metabolism. Chembiochem 26(7):e202401086.
[43] Buescher, J.M., Antoniewicz, M.R., Boros, L.G., Burgess, S.C., Brunengraber, H., Clish, C.B., et al., 2015. A roadmap for interpreting 13C metabolite labeling patterns from cells. Current opinion in biotechnology 34:189-201.
[44] Christen, S., Lorendeau, D., Schmieder, R., Broekaert, D., Metzger, K., Veys, K., et al., 2016. Breast cancer-derived lung metastases show increased pyruvate carboxylase-dependent anaplerosis. Cell reports 17(3):837-848.
[45] Bruntz, R.C., Lane, A.N., Higashi, R.M., Fan, T.W.-M., 2017. Exploring cancer metabolism using stable isotope-resolved metabolomics (SIRM). Journal of Biological Chemistry 292(28):11601-11609.
[46] Johnston, K., Pachnis, P., Tasdogan, A., Faubert, B., Zacharias, L.G., Vu, H.S., et al., 2021. Isotope tracing reveals glycolysis and oxidative metabolism in childhood tumors of multiple histologies. Med 2(4):395-410. e394.
[47] Lau, A.N., Li, Z., Danai, L.V., Westermark, A.M., Darnell, A.M., Ferreira, R., et al., 2020. Dissecting cell-type-specific metabolism in pancreatic ductal adenocarcinoma. Elife 9:e56782.
[48] Pachnis, P., Wu, Z., Faubert, B., Tasdogan, A., Gu, W., Shelton, S., et al., 2022. In vivo isotope tracing reveals a requirement for the electron transport chain in glucose and glutamine metabolism by tumors. Science Advances 8(35):eabn9550.
[49] Holm, L.J., Haupt-Jorgensen, M., Larsen, J., Giacobini, J.D., Bilgin, M., Buschard, K., 2018. L-serine supplementation lowers diabetes incidence and improves blood glucose homeostasis in NOD mice. PLoS ONE 13(3):e0194414.
[50] Lopez-Gonzales, E., Lehmann, L., Ruiz-Ojeda, F.J., Hernandez-Bautista, R., Altun, I., Onogi, Y., et al., 2022. L-Serine Supplementation Blunts Fasting-Induced Weight Regain by Increasing Brown Fat Thermogenesis. Nutrients 14(9).
[51] Handzlik, M.K., Metallo, C.M., 2023. Sources and Sinks of Serine in Nutrition, Health, and Disease. Annu Rev Nutr 43:123-151.
[52] Achouri, Y., Robbi, M., Van Schaftingen, E., 1999. Role of cysteine in the dietary control of the expression of 3-phosphoglycerate dehydrogenase in rat liver. Biochem J 344 Pt 1:15-21.
[53] Garcia, R.A., Stipanuk, M.H., 1992. The splanchnic organs, liver and kidney have unique roles in the metabolism of sulfur amino acids and their metabolites in rats. J Nutr 122(8):1693-1701.
[54] Stipanuk, M.H., Coloso, R.M., Garcia, R.A., Banks, M.F., 1992. Cysteine concentration regulates cysteine metabolism to glutathione, sulfate and taurine in rat hepatocytes. J Nutr 122(3):420-427.
[55] Coloso, R.M., Hirschberger, L.L., Stipanuk, M.H., 1991. Uptake and metabolism of L-2-oxo-[35S]thiazolidine-4-carboxylate by rat cells is slower than that of L-[35S]cysteine or L-[35S]methionine. J Nutr 121(9):1341-1348.

[56] Bagley, P.J., Stipanuk, M.H., 1995. Rats fed a low protein diet supplemented with sulfur amino acids have increased cysteine dioxygenase activity and increased taurine production in hepatocytes. J Nutr 125(4):933-940.
[57] Farrera, D.O., Galligan, J.J., 2022. The Human Glyoxalase Gene Family in Health and Disease. Chem Res Toxicol.
[58] Trujillo, M.N., Jennings, E.Q., Hoffman, E.A., Zhang, H., Phoebe, A.M., Mastin, G.E., et al., 2024. Lactoylglutathione promotes inflammatory signaling in macrophages through histone lactoylation. Mol Metab:101888.
[59] Xin, C., Cai, M., Jia, Q., Huang, R., Li, R., Wang, J., et al., 2025. Dietary sulfur amino acid restriction improves metabolic health by reducing fat mass. Life Metab 4(3):loaf009.
[60] Krall, A.S., Xu, S., Graeber, T.G., Braas, D., Christofk, H.R., 2016. Asparagine promotes cancer cell proliferation through use as an amino acid exchange factor. Nat Commun 7:11457.
[61] Hasek, B.E., Boudreau, A., Shin, J., Feng, D., Hulver, M., Van, N.T., et al., 2013. Remodeling the integration of lipid metabolism between liver and adipose tissue by dietary methionine restriction in rats. Diabetes 62(10):3362-3372.
[62] Badenhorst, C.P.S., van der Sluis, R., Erasmus, E., Van Dijk, A.A., 2013. Glycine conjugation: importance in metabolism, the role of glycine N-acyltransferase, and factors that influence interindividual variation. Expert opinion on drug metabolism & toxicology 9(9):1139-1153.

FIGURE CAPTIONS

Figure 1. Sulfur amino acid restriction (SAAR) prevents obesity and improves systemic glucose control in C57BL/6J mice. A. A schematic representation of the study design. C57BL/6J male mice were fed a low-fat control (LF-CTRL), high-fat control (HF-CTRL), or HF-SAAR diet for 6 weeks starting at 6 weeks of age. **B.** Body weight time course (g), body weight change over the 6 weeks on diet (g), fat mass (% of body weight), and lean mass (% of body weight). **C.** Liver triglycerides ($mg \cdot g^{-1}$) and liver weight (g). **D.** Liver glycogen ($mg \cdot g^{-1}$)**. E.** Blood glucose ($mg \cdot dL^{-1}$). **F.** Glucose excursion and area under the curve (AUC) during a glucose tolerance test. **G.** Glucose excursion and AUC during an insulin tolerance test. **H.** Plasma insulin ($pmol \cdot L^{-1}$). n=3-17. *$p<0.05$, **$p<0.01$, ***$p<0.001$, ****$p<0.0001$.

Figure 2. Sulfur amino acid restriction (SAAR) increases liver glucose partitioning to *de novo* serine synthesis in C57BL/6J mice. A. A schematic representation of the select reactions involved in *de novo* serine synthesis and SAA synthesis and catabolism. **B.** Liver methionine, cysteine, and taurine (arbitrary units) in C57BL/6J male mice fed a low-fat control (LF-CTRL), high-fat control (HF-CTRL), or HF-SAAR diet for 6 weeks starting at 6 weeks of age. **C.** Liver phosphoglycerate dehydrogenase (PHGDH) and phosphoserine aminotransferase 1 (PSAT1) as determined by immunoblotting and representative immunoblots in mice fed a LF-CTRL, HF-CTRL, and HF-SAAR diet. **D.** Liver PSAT1 as determined by immunoblotting and representative immunoblots in mice fed a LF-CTRL and HF-CTRL diet only. **E.** Liver serine and glycine (arbitrary units). **F.** A schematic representation of the study design. C57BL/6J mice were fed a LF-CTRL (0.88% kcal from methionine, 510072, Dyets Inc., Bethlehem, PA) or low-fat SAAR (LF-SAAR; 0.18% kcal from methionine, 510071, Dyets Inc., Bethlehem, PA) for 6 weeks starting at 6 weeks of age. See

790 Supplementary Table 3 for diet details. A 30-minute intravenous infusion of [U-^{13}C]glucose in the
791 conscious, unrestrained mouse was completed at 12 weeks of age. **G.** Arterial blood glucose
792 (mg·dL^{-1}). **H.** Fractional enrichment (% total pool) of liver glucose, serine and glycine from [U-
793 ^{13}C]glucose. n=6-10. $^{\#}$p<0.05 by *t*-test, *p<0.05, **p<0.01, ***p<0.001, ****p<0.0001 by
794 ANOVA.
795
796
797 **Figure 3. Liver PSAT1 is required for systemic glucose adaptations to sulfur amino acid**
798 **restriction (SAAR). A.** A schematic representation of the study design. Liver-specific PSAT1
799 knockout (KO) mice and wild type (WT) littermates were fed a high-fat control (HF-CTRL) or
800 HF-SAAR diet for 6 weeks. **B.** Body weight time course (g) and body weight change over 6 weeks
801 on diet (g). **C.** Fat mass and lean mass (% of body weight). **D.** Glucose excursion curves and area
802 under the curve (AUC) for glucose tolerance tests. **E.** Glucose excursion curves and AUC for
803 insulin tolerance tests. **F.** Plasma insulin (pmol·L^{-1}) before (0 min) and 15 minutes after an insulin
804 injection. **G.** Liver phosphor-Akt (p-Akt)-to-Akt ratio as determined by immunoblotting and
805 representative immunoblots. **H.** Liver glycogen (mg·g^{-1}). **I.** Liver phospho-glycogen synthase (p-
806 GS)-to-GS ratio and phospho-glycogen phosphorylase (p-PYGL)-to-PYGL ratio as determined by
807 immunoblotting and representative immunoblots. n=5-18. *p<0.05, **p<0.01, ***p<0.001,
808 ****p<0.0001.
809
810
811 **Figure 4. Sulfur amino acid restriction (SAAR) increases liver *de novo* serine synthesis from**
812 **glucose. A.** A schematic representation of select metabolites and enzymes involved in *de novo*
813 serine synthesis from glucose. **B.** Liver phosphoglycerate dehydrogenase (PHGDH),
814 phosphoserine aminotransferase 1 (PSAT1), and serine hydroxymethyltransferase 2 (SHMT2) as
815 determined by immunoblotting and representative immunoblots in wild type (WT) and liver-
816 specific PSAT1 knockout (KO) mice fed a high-fat control (HF-CTRL) or HF-SAAR diet for 6
817 weeks. **C.** Liver glucose, serine, and glycine (arbitrary units) in 7-hour fasted mice. **D.** Fractional
818 enrichment (% of total pool) of liver glucose, serine, and glycine following a 30-minute
819 intravenous infusion of [U-^{13}C]glucose. n=7-9. *p<0.05, **p<0.01, ***p<0.001, ****p<0.0001.
820
821
822 **Figure 5. Sulfur amino acid restriction (SAAR) increases partitioning of glucose-sourced**
823 **serine to liver glutathione. A.** A schematic representation of the select reactions involved in *de*
824 *novo* serine synthesis and SAA synthesis and catabolism. **B.** Liver cystathionine β-synthase (CBS),
825 cystathionine γ-lyase (CSE), cysteine dioxygenase 1 (CDO1), glutamate-cysteine ligase catalytic
826 subunit (GCLC), and glutathione synthetase (GSS) as determined by immunoblotting and
827 representative immunoblots in wild type (WT) and liver-specific PSAT1 knockout (KO) mice fed
828 a high-fat control (HF-CTRL) or HF-SAAR diet for 6 weeks. **C.** Liver methionine, cysteine,
829 taurine, reduced glutathione (GSH), and oxidized glutathione (GSSG; arbitrary units) in 7-hour
830 fasted mice. **D.** Fractional enrichment (% of total pool) of liver methionine, taurine, GSH, and
831 GSSG following a 30-minute intravenous infusion of [U-^{13}C]glucose. **E.** Fractional enrichment
832 (% of total pool) of liver serine, methionine, taurine, GSH, and GSSG at 15 minutes following an
833 i.p. injection of [U-^{13}C]serine. n=6-9. *p<0.05, **p<0.01, ***p<0.001, ****p<0.0001.
834

835
836 **Figure 6. Sulfur amino acid restriction (SAAR) lowers glyoxalase cycle metabolites and**
837 **associated post-translational modifications (PTMs). A.** A schematic of select reactions,
838 metabolites, and PTMs related to the glyoxalase cycle. **B.** Liver glyoxalase 1 (GLO1) and
839 hydroxyacylglutathione hydrolase (GLO2) as determined by immunoblotting and representative
840 immunoblots in wild type (WT) and liver-specific PSAT1 knockout (KO) mice fed a high-fat
841 control (HF-CTRL) or HF-SAAR diet for 6 weeks. **C.** Liver glutathione (GSH; arbitrary units),
842 hemithioacetal (HTA; arbitrary units), lactoylglutathione (arbitrary units), and lactate (arbitrary
843 units). **D.** Global PTMs (pmol·nmol Leu^{-1}): lactoyllysine, methylglyoxal-derived
844 hydroimidazolone 1 (MG-H1), carboxyethylarginine (CEA), and acetyllysine. n=6-9. *p<0.05,
845 **p<0.01, ****p<0.0001.
846
847
848 **Figure 7. Sulfur amino acid restriction (SAAR) increases glucose partitioning toward**
849 **asparagine synthesis. A.** A schematic representation of select reactions and metabolites linking
850 tricarboxylic acid (TCA)-cycle intermediates to asparagine synthesis. **B.** Liver TCA cycle,
851 anaplerotic and cataplerotic metabolites (arbitrary units) in wild type (WT) and liver-specific
852 PSAT1 knockout (KO) mice fed a high-fat control (HF-CTRL) or HF-SAAR diet for 6 weeks. **C.**
853 Fractional enrichment (% of total pool) of liver TCA cycle, anaplerotic and cataplerotic metabolites
854 following a 30-minute intravenous infusion of [U-^{13}C]glucose. **D.** Ratios of isotopologues used as
855 indices of anaplerotic and cataplerotic flux. **E.** Liver asparagine synthase (ASNS), pyruvate
856 carboxylase (PC), propionyl-CoA carboxylase subunit A (PCCA), malate dehydrogenase 2
857 (MDH2), and mitochondrial glutamic-oxaloacetic transaminase (GOT2) as determined by
858 immunoblotting and representative immunoblots. n=6-9. *p<0.05, **p<0.01, ***p<0.001,
859 ****p<0.0001.
860
861
862 **Figure 8. Sulfur amino acid restriction (SAAR) reduces lipid accumulation independently of**
863 **hepatic PSAT1.** Panels A-G are measurements in in wild type (WT) and liver-specific PSAT1
864 knockout (KO) mice fed a high-fat control (HF-CTRL) or HF-SAAR diet for 6 weeks. Panels H-
865 J are measurements in WT and KO mice fed the HF-CTRL and -SAAR diets for 20 weeks. **A.**
866 Liver triglycerides (mg·g^{-1}). **B.** Liver *de novo* lipogenesis enzymes: ATP-citrate lyase (ACLY),
867 acetyl-CoA carboxylase (ACC), fatty acid synthase (FASN), and stearoyl-CoA desaturase 1
868 (SCD1) as determined by immunoblotting (arbitrary units). **C.** Liver mitochondrial respiratory
869 complexes I-V (CI-V) as determined by immunoblotting. **D.** Representative immunoblots for
870 panels B, C, and F. **E.** A schematic representation of select metabolites and enzymes related to the
871 synthesis of acylglycines. **F.** Liver glycine N-acyltransferase (GLYAT) as determined by
872 immunoblotting. **G.** Liver acylglycines (arbitrary units): acetylglycine, isobutyrylglycine,
873 isovalerylglycine, hexanoylglycine, and capryloylglycine. **H.** Body weight time course (g) and
874 change in body weight (g) over 20 weeks on diet. **I.** Fat mass and lean mass (% body weight).
875 **J.** Liver triglycerides (mg·g^{-1}). n=5-9 *p<0.05, **p<0.01, ***p<0.001, ****p<0.0001.
876
877
878 **Supplementary Figure 1. Sulfur Amino Acid Restriction (SAAR) impacts systemic glucose**
879 **control and hepatic glucose partitioning in C57BL/6J mice independent of insulin levels. A.**
880 A schematic representation of the study design. C57BL/6J male mice were fed a low-fat control

881 (LF-CTRL), high-fat control (HF-CTRL), or HF-SAAR diet for 6 weeks starting at 6 weeks of
882 age. A subset of mice fed the HF-SAAR diet had a subcutaneous insulin pellet (HF-SAAR +
883 Insulin) implanted at 7 weeks of age for sustained release of insulin until 12 weeks of age. **B.** Body
884 weight time course (g), body weight change over the 6 weeks on diet (g), fat mass (% of body
885 weight), and lean mass (% of body weight). **C.** Liver triglycerides ($mg \cdot g^{-1}$) and liver weight (g). **D.**
886 Liver glycogen ($mg \cdot g^{-1}$). **E.** Blood glucose ($mg \cdot dL^{-1}$). **F.** Glucose excursion and area under the
887 curve (AUC) during a glucose tolerance test. **G.** Glucose excursion and AUC during an insulin
888 tolerance test. **H.** Plasma insulin ($pmol \cdot L^{-1}$). **I.** Liver methionine, homocysteine, cysteine, and
889 taurine (arbitrary units). **J.** Liver phosphoglycerate dehydrogenase (PHGDH) and phosphoserine
890 aminotransferase 1 (PSAT1) as determined by immunoblotting and representative
891 immunoblots. **K.** Liver serine and glycine (arbitrary units). n=3-17. $^{\#}p<0.05$ by *t*-test. $^{*}p<0.05$,
892 $^{**}p<0.01$, $^{***}p<0.001$, $^{****}p<0.0001$ by ANOVA.

Graphical Abstract. Schematic representation of liver glucose adaptations to SAAR

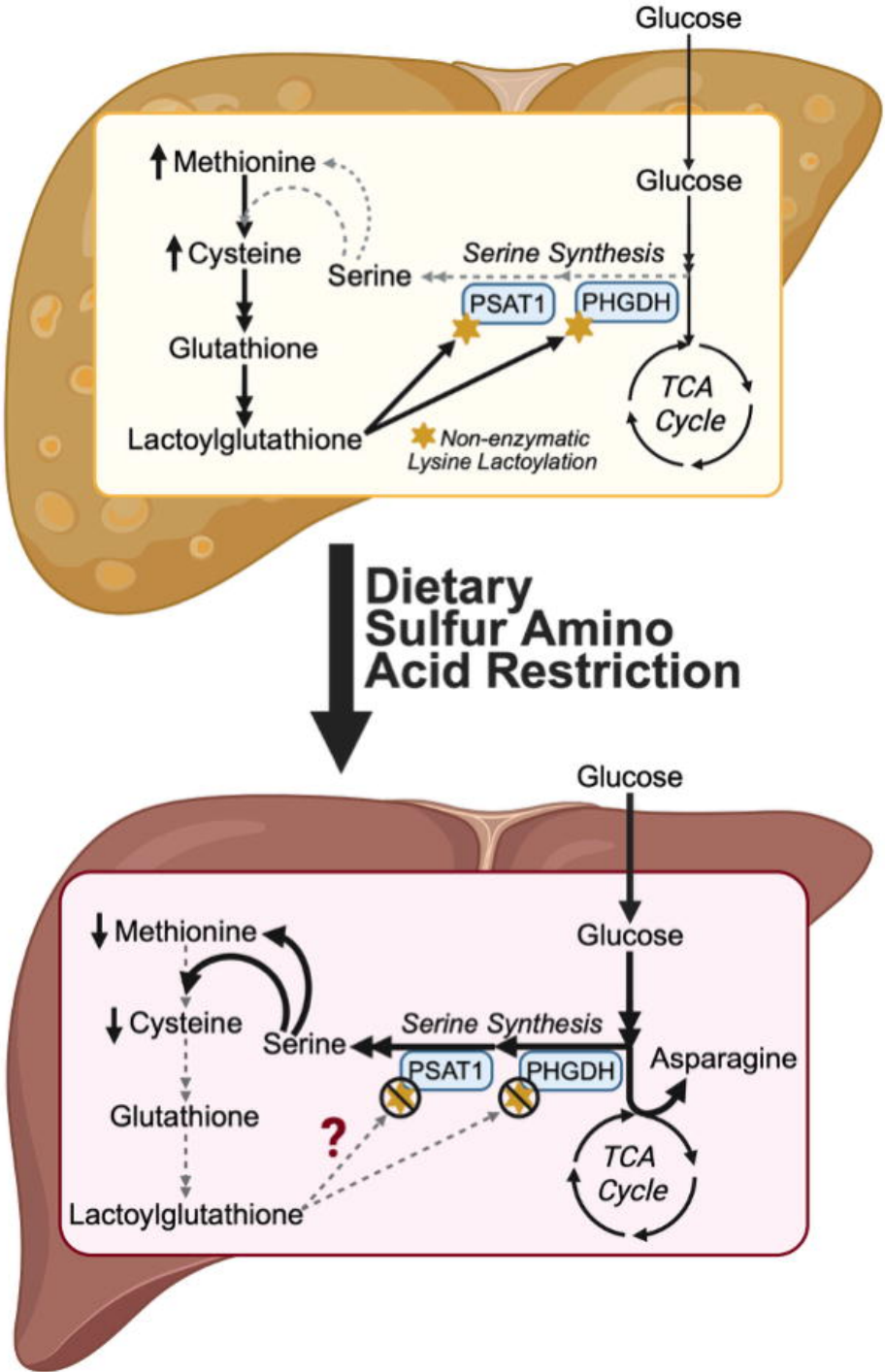

Figure 1. SAAR prevents obesity and improves systemic glucose control in C57BL/6J mice

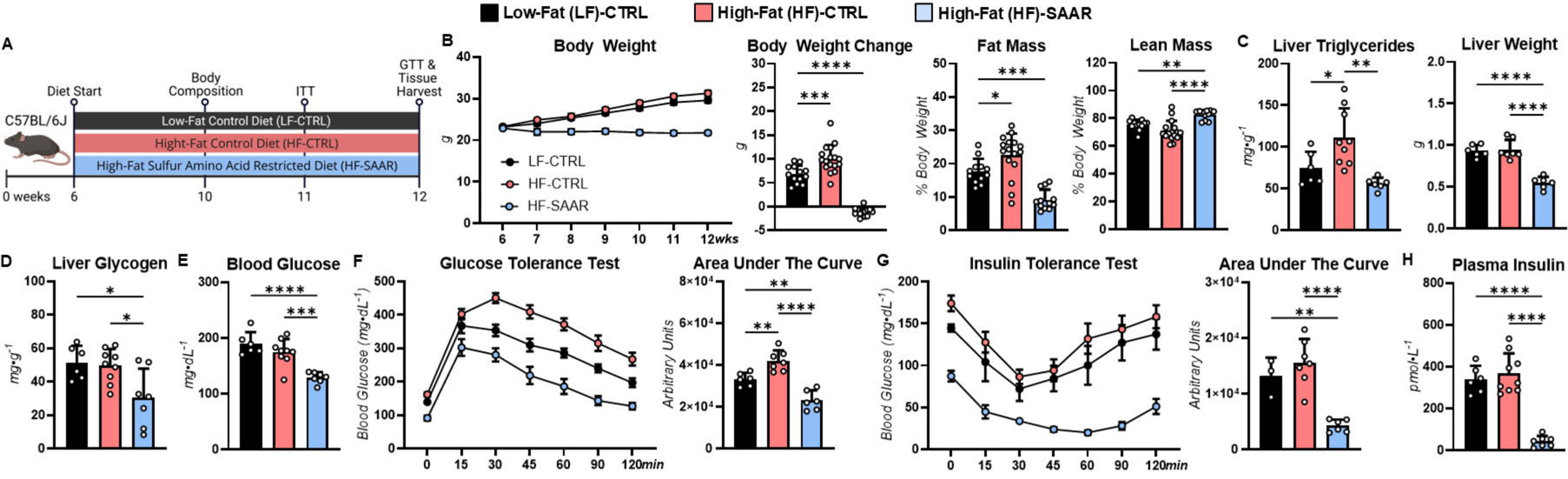

Figure 2. SAAR increased glucose partitioning to de novo serine synthesis in C57BL/6J mice

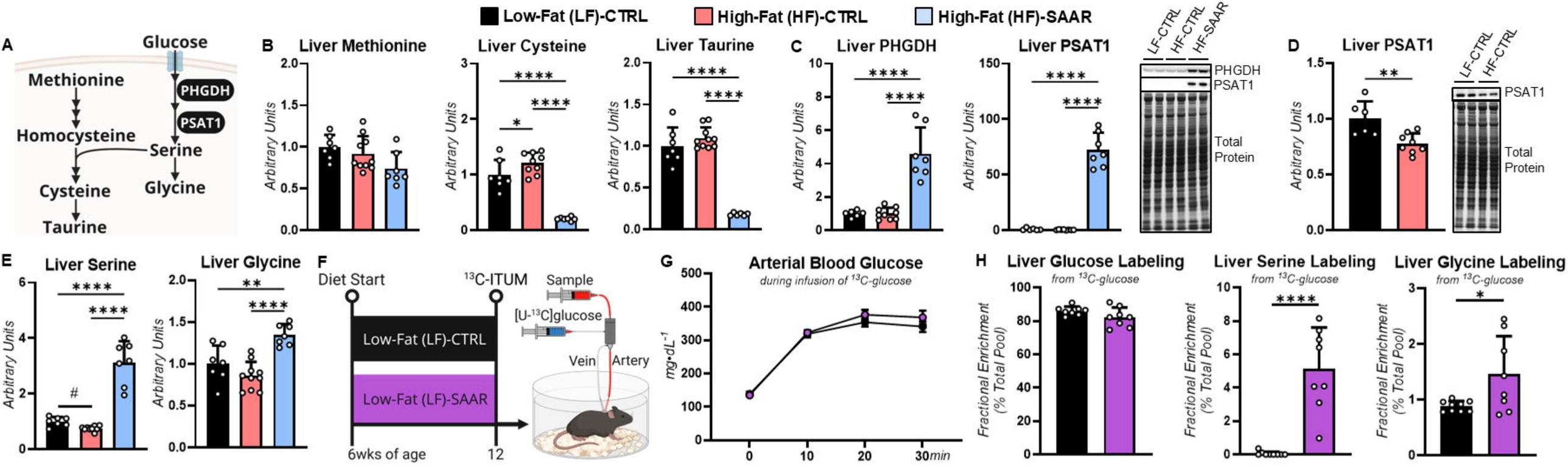

Figure 3. Liver PSAT1 is required for systemic glucose adaptations to SAAR

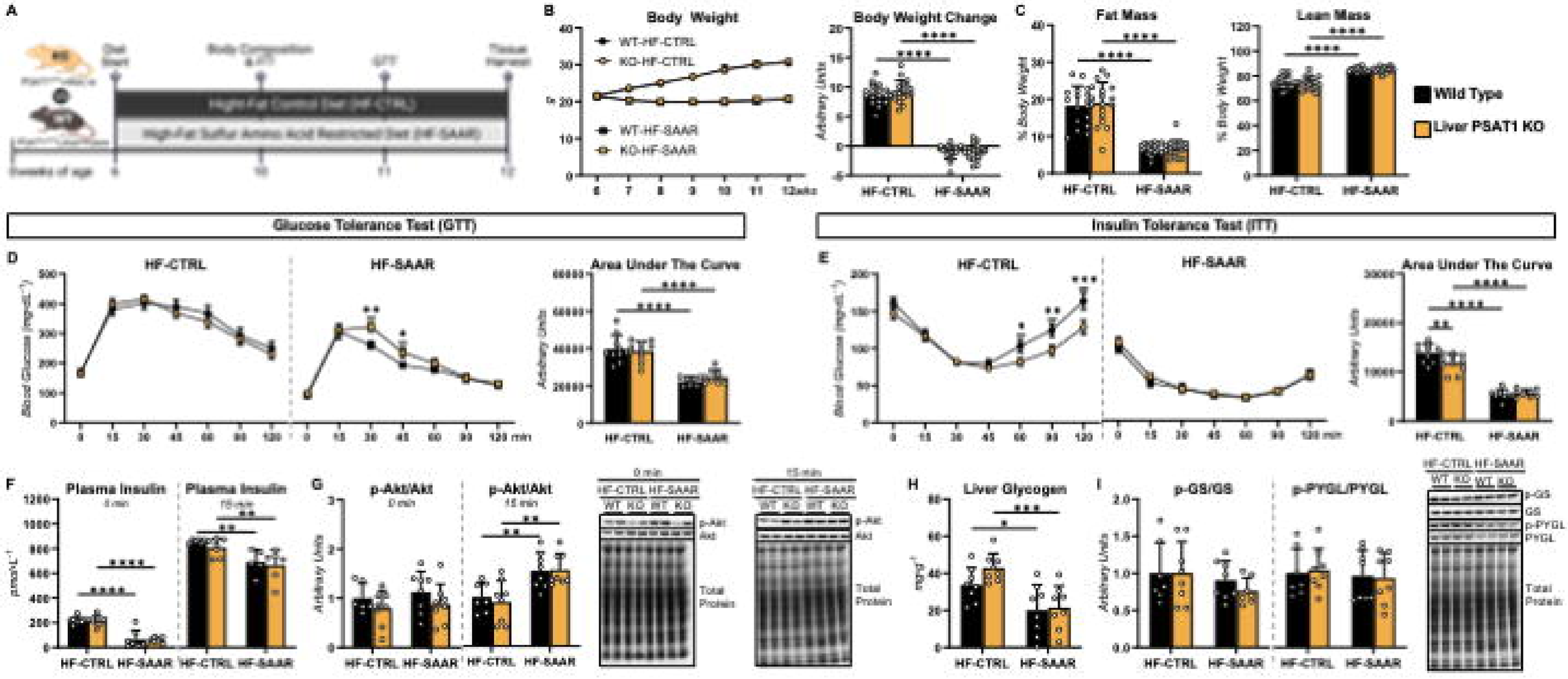

Figure 4. SAAR increases liver de novo serine synthesis from glucose

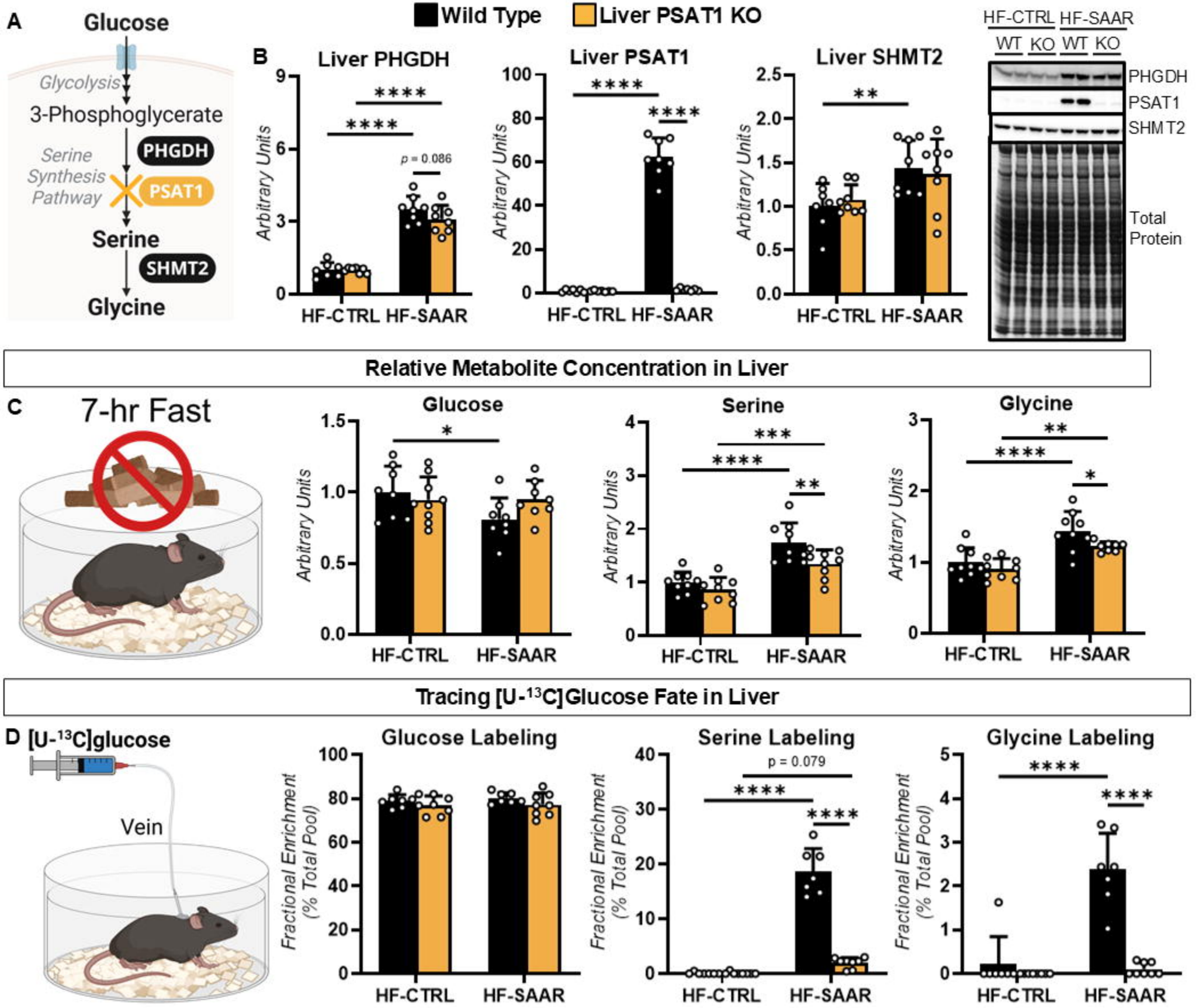

Figure 5. SAAR increases partitioning of glucose-sourced serine to glutathione

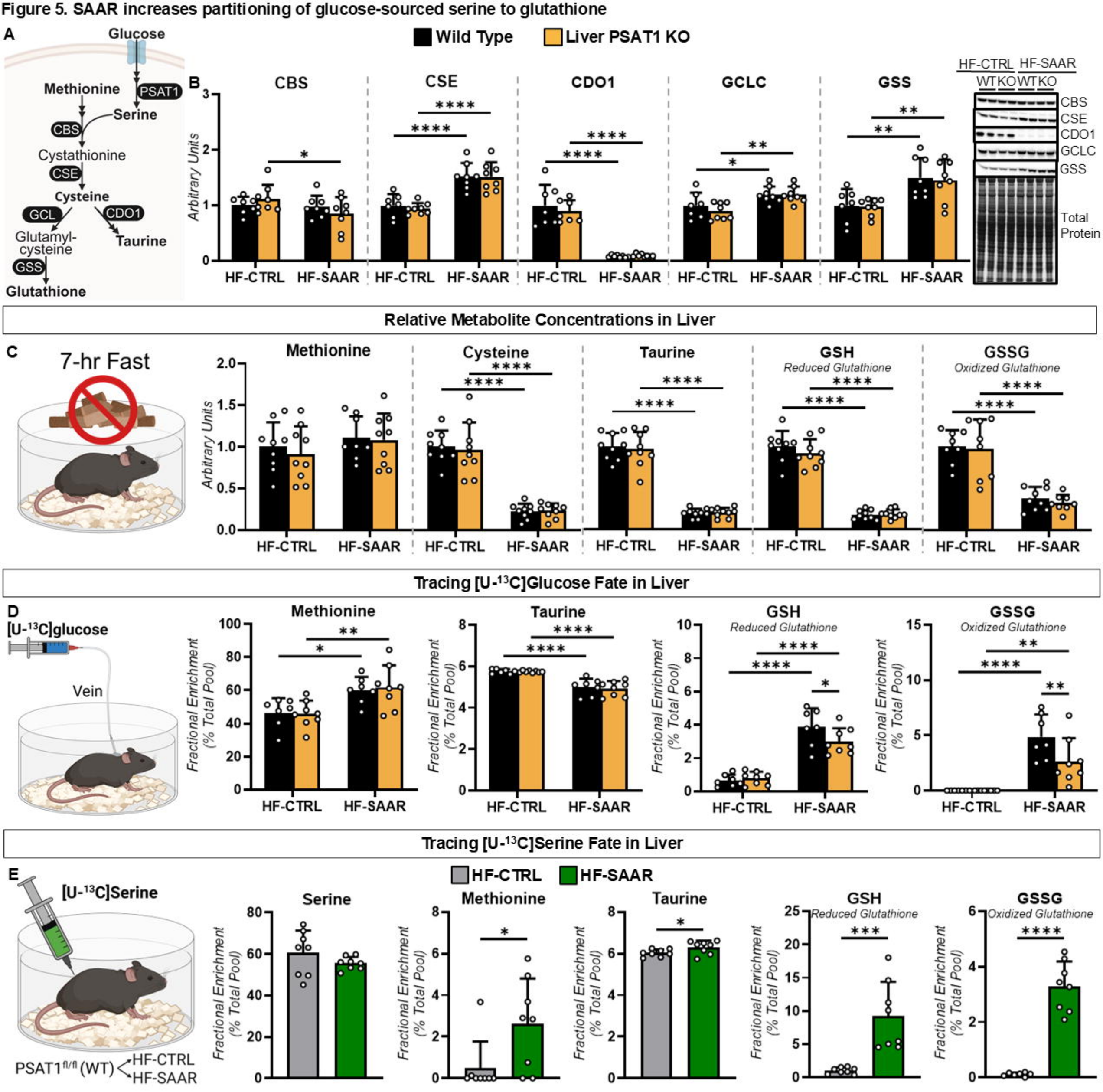

Figure 6. SAAR lowers liver glyoxalase cycle metabolites and associated post-translational modifications

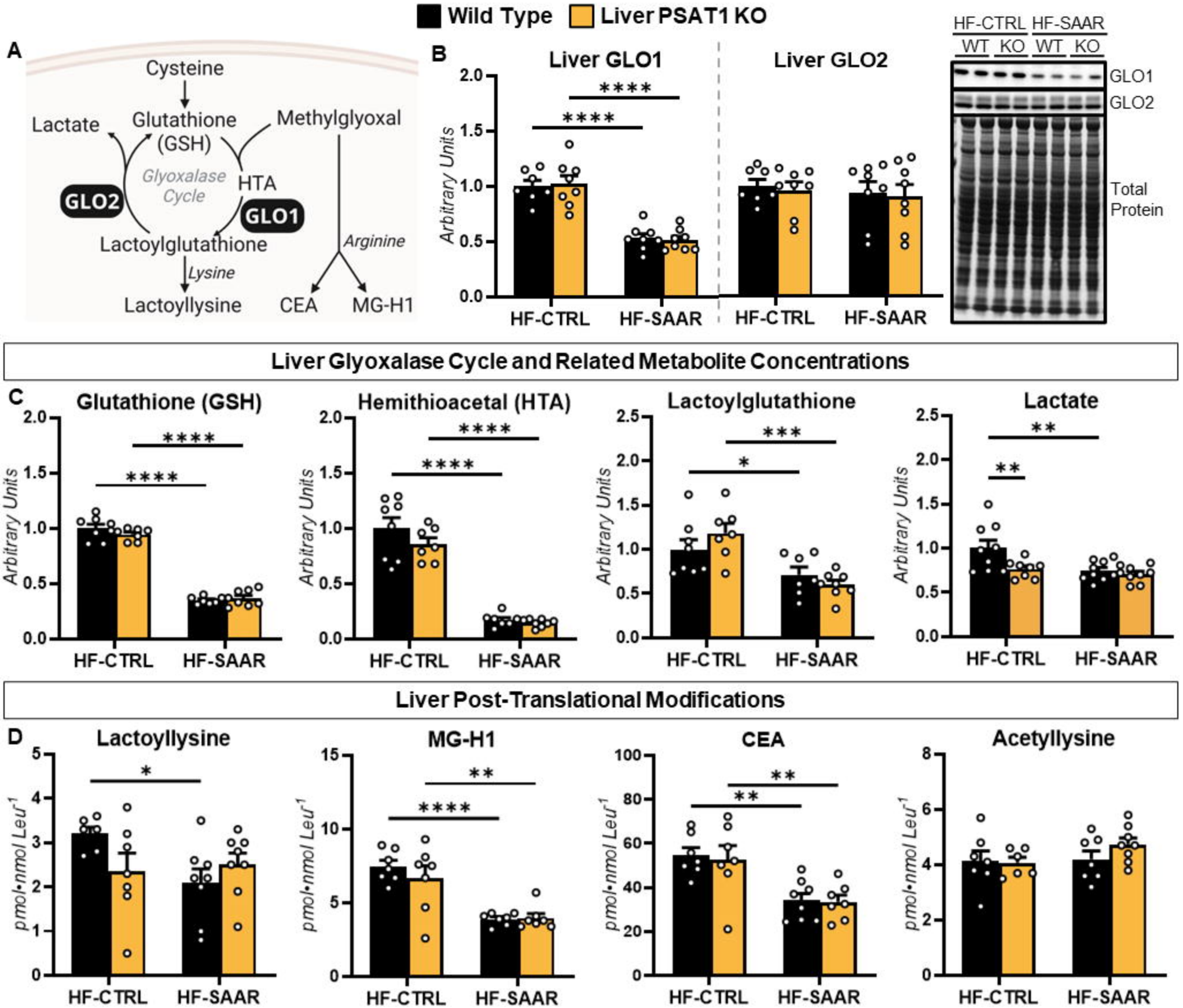

Figure 7. SAAR increased glucose partitioning toward liver asparagine synthesis

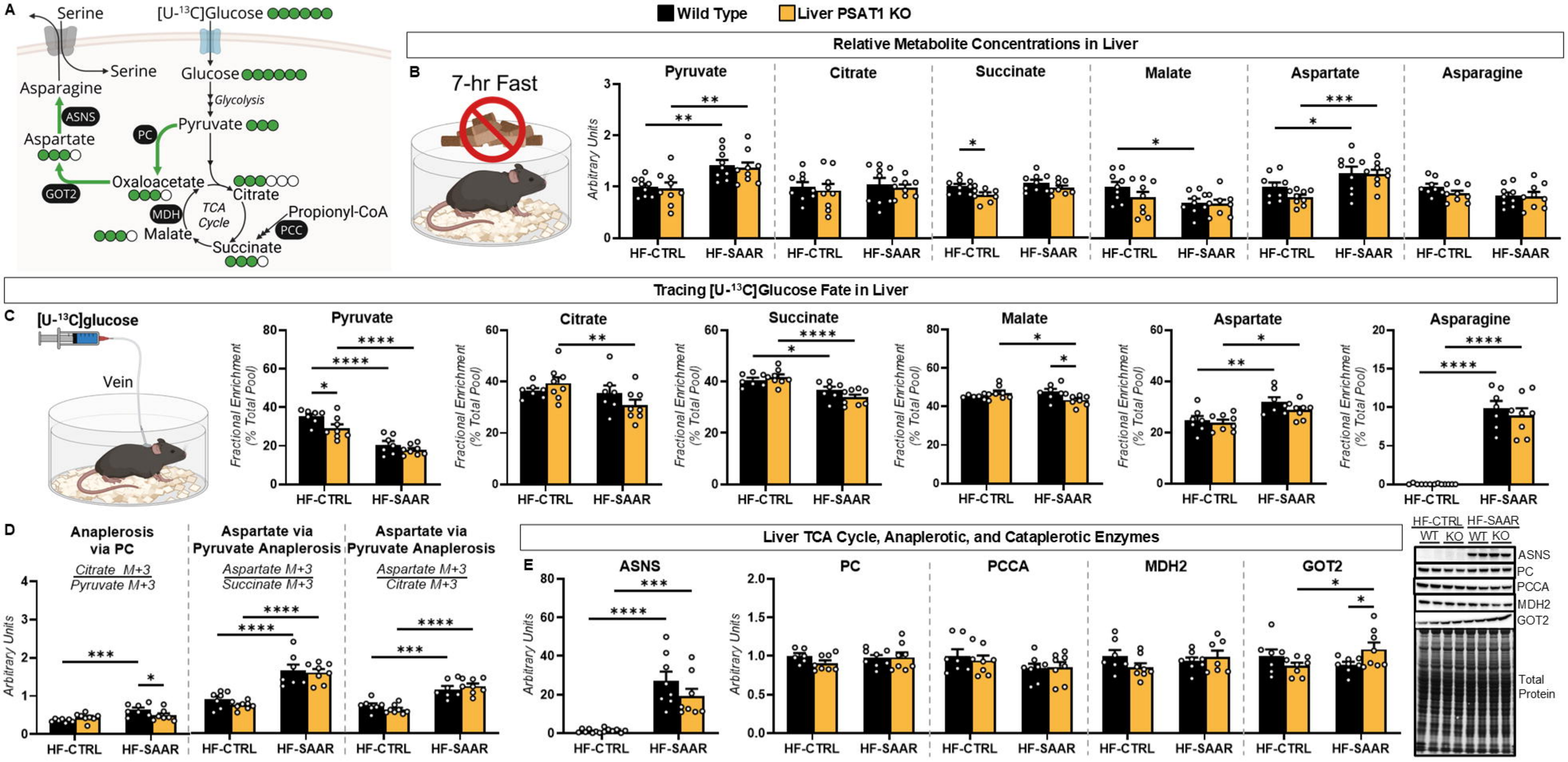
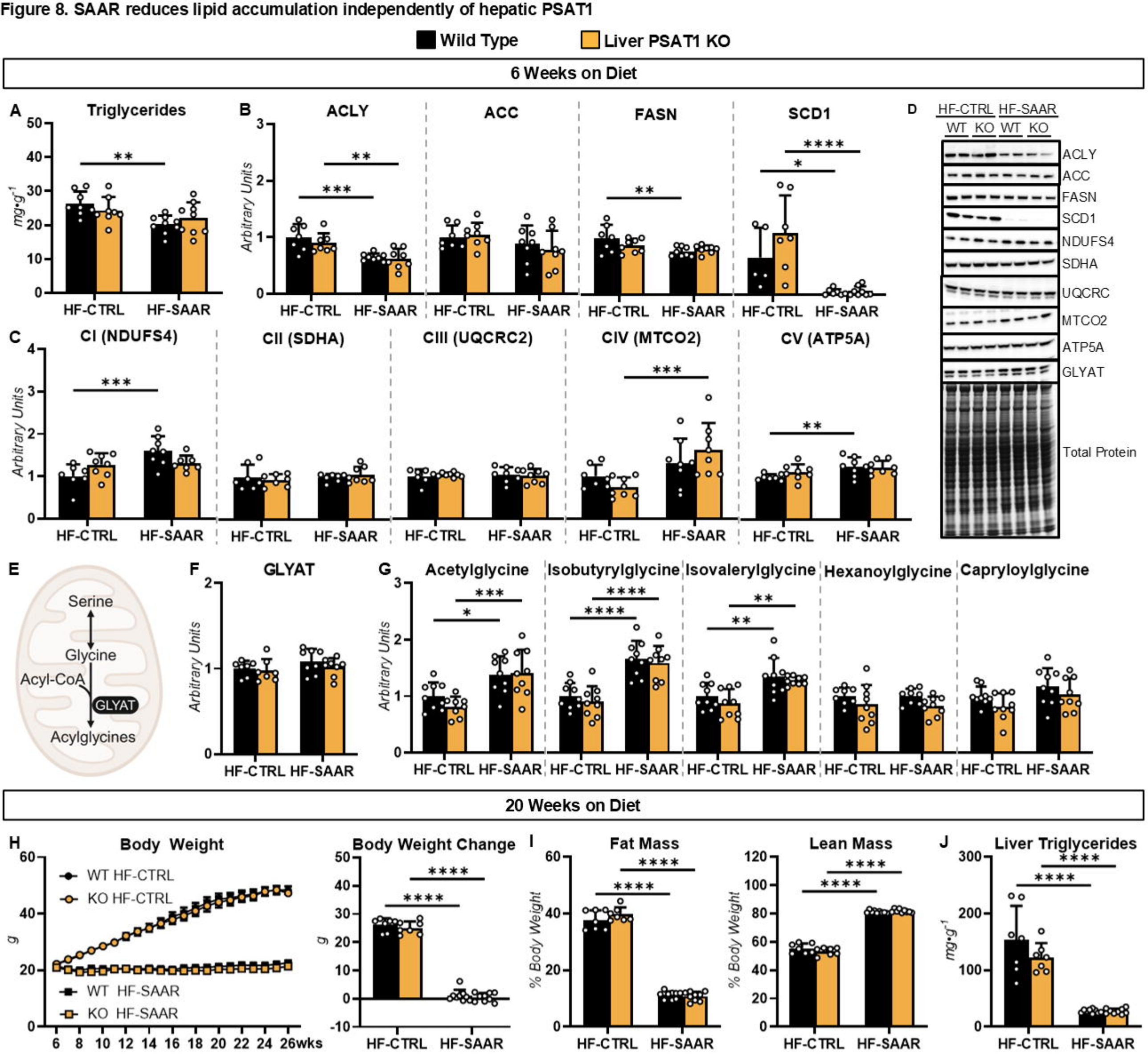
Figure 8. SAAR reduces lipid accumulation independently of hepatic PSAT1